Contract No. DTFACT-15-D-00007
Construction Cycle 8: Phase I Test Report
DELIVERABLE 4.9.2

February 2017

Prepared by Dr. Hao Yin, Gemini Technologies, Inc.

Submitted by SRA International, Inc., a CSRA Company

2/2017

TABLE OF CONTENTS

LIST OF FIGURES

LIST OF TABLES

LIST OF ACRONYMS

2D	Dual Tandem
AC	Advisory Circular
CC6	Construction Cycle 6
CC8	Construction Cycle 8
CAN-PCN	Aircraft Classification Number–Pavement Classification Number
CDF	Cumulative Damage Factor
D	Dual
ECS	Eddy Current Sensor
EG	Embedded Strain Gage
FAA	Federal Aviation Administration
HWD	Heavy Falling-Weight Deflectometer
ICAO	International Civil Aviation Organization
NAPTF	National Airport Pavement Test Facility
SCI	Structural Condition Index
PCC	Portland Cement Concrete
POT	Potentiometer
PSPA	Portable Seismic Pavement Analyzer

EXECUTIVE SUMMARY

As part of Construction Cycle 8 (CC8) at the National Airport Pavement Test Facility (NAPTF), the Federal Aviation Administration (FAA) is conducting full-scale tests on an unbonded concrete overlay test pavement. In preparation for receiving the portland cement concrete (PCC) overlay, the relatively thin existing PCC surface layer was damaged by simulated heavy aircraft gear traffic applied by the NAPTF test vehicle. Data obtained from this initial trafficking phase will be used by the FAA to evaluate current International Civil Aviation Organization (ICAO) standards for allowable aircraft overloads on rigid pavements. This paper discusses various aspects of the overload testing, including: pavement design, construction, and instrumentation, PCN evaluation, overload test procedures, and traffic test results. The difference in applied coverages to failure was used to evaluate the effect of the overload. In addition, the cause and failure mechanism of observed distresses were discussed. This overload test generated a unique full-scale test data set, which be used by the FAA to evaluate current ICAO standards for allowable aircraft overloads on rigid pavements.

1. INTRODUCTION

The Aircraft Classification Number–Pavement Classification Number (ACN–PCN) system of rating airport pavements is designated by the International Civil Aviation Organization (ICAO) as the only approved method for reporting pavement strength. ACN is a number that expresses the relative effect of an aircraft at a given configuration on a pavement structure for a specified standard subgrade strength. PCN is a number that expresses the load-carrying capacity of a pavement for unrestricted operations. The concept of ACN-PCN method is structured so that a pavement with a given PCN value can support unrestricted operations of an aircraft that has an ACN value equal to or less than the PCN value. FAA Advisory Circular (AC) 150/5335-5C (FAA 2014) provides guidance on reporting airport pavement strength and is mandatory for all projects funded with federal grant money through the AIP program. ICAO Annex 14 (ICAO 2013) establishes overload criteria for both rigid and flexible airport pavements. The ICAO criteria recognize that airport operators should have flexibility to allow occasional operations by aircraft whose ACN exceeds the assigned PCN, and that as long as these operations do not become regular, the additional damage they cause is likely to be manageable. As stated in AC 150/5335-5C, Appendix D, "With the exception of massive overloading, pavements do not suddenly or catastrophically fail. As a result, occasional minor overloading is acceptable with only limited loss of pavement life expectancy and relatively small acceleration of pavement deterioration." According to ICAO Annex 14, occasional movements on rigid pavements by aircraft with ACN values not exceeding 5 percent above the reported PCN "should not adversely affect the pavement."

2. RESEARCH SIGNIFICANCE

The objective of the research effort was to develop new, rational overload criteria for airfield rigid pavements. Although the current ICAO overload criteria represent a "reasonable balance between operational flexibility and the need to avoid undue damage to pavements," (Defence Estates 2011) they are still somewhat conservative and unsupported by empirical data. For example, limited Construction Cycle 6 (CC6) test data at the FAA's NAPTF demonstrated that a one-time application of rupture load (i.e., equal to or exceeding the slab strength) did not necessarily shorten pavement life (Brill 2013). Ideally, allowable overload criteria would be linked to the cumulative damage factor (CDF), which would then allow individual overloads to be related to consumed life.

3. TEST PAVEMENT AND INSTRUMENTATION

The FAA is conducting full-scale tests on an unbonded concrete overlay test pavement, designated CC8, at the NAPTF. In preparation for receiving the PCC overlay, the relatively thin existing PCC surface layer was damaged by simulated heavy aircraft gear traffic applied by the NAPTF test vehicle. The overload test area has two test items (north and south), is 60 feet long by 60 feet wide, and consists of twenty 12×12-ft. slabs, as shown in figure 1. The pavement structure is 9-inch thick concrete slabs on an 11-inch thick granular base, on a prepared clay subgrade. Based on plate load tests, the modulus of subgrade reaction (*k*-value) is approximately 110 pci on the north test item, and 131 pci on the south test item. Since no stabilized base is present, this rigid pavement structure may be considered representative of a non-hub or general aviation facility, i.e., not intended to handle heavy aircraft loads. All longitudinal joints are

doweled and all dowels are 0.75 inches in diameter. However, the transverse joints are not doweled.

Prior to the placement of the surface P-501 layer, all subgrade, subbase and concrete slab instrumentation had to be installed. The selection of gages was based on reliability, accuracy, price, and ease of handling at the construction site. Instrumentation details are given in figure 1. Vertical movement of slab corners relative to the base was monitored by both potentiometers (POTs) and eddy current sensors (ECS). Because previous experience showed that POTs may be susceptible to damage from water intrusion, a special watertight housing was devised. At installation, a steel plate was first anchored into the subbase to serve as a stationary reference point. The POT assembly was then installed as shown in figure 2. A rebar chair was used to secure the height of the POT at its mid-travel position as the slab was constructed. This was done to ensure that both up and down movement relative to the initial position could be recorded. Figure 2 also shows the ECS with protruding bolts to anchor it in the concrete. Both POTs and ECSs are intended to operate in static mode (to monitor long-term upward movement of slab corners) and dynamic mode (to record transient responses to vehicle loads). Pairs of embedded strain gages were installed along longitudinal and transverse edges of eight slabs to measure strain responses near the top (odd numbered gages) and bottom (even numbered gages) of the instrumented slabs. Rebar chairs ensured that strain gages were set at the proper height (1 in. above the slab bottom and 1 in. below the slab top). Thermocouple trees were installed in two slabs to monitor slab temperature gradients. Each tree consists of three thermocouples to measure temperature at the bottom, middle, and top of the slab. In addition, moisture sensors were installed at two locations to monitor the subgrade soil moisture content. These sensors were located 6 inches below the subgrade surface during the subgrade preparation.

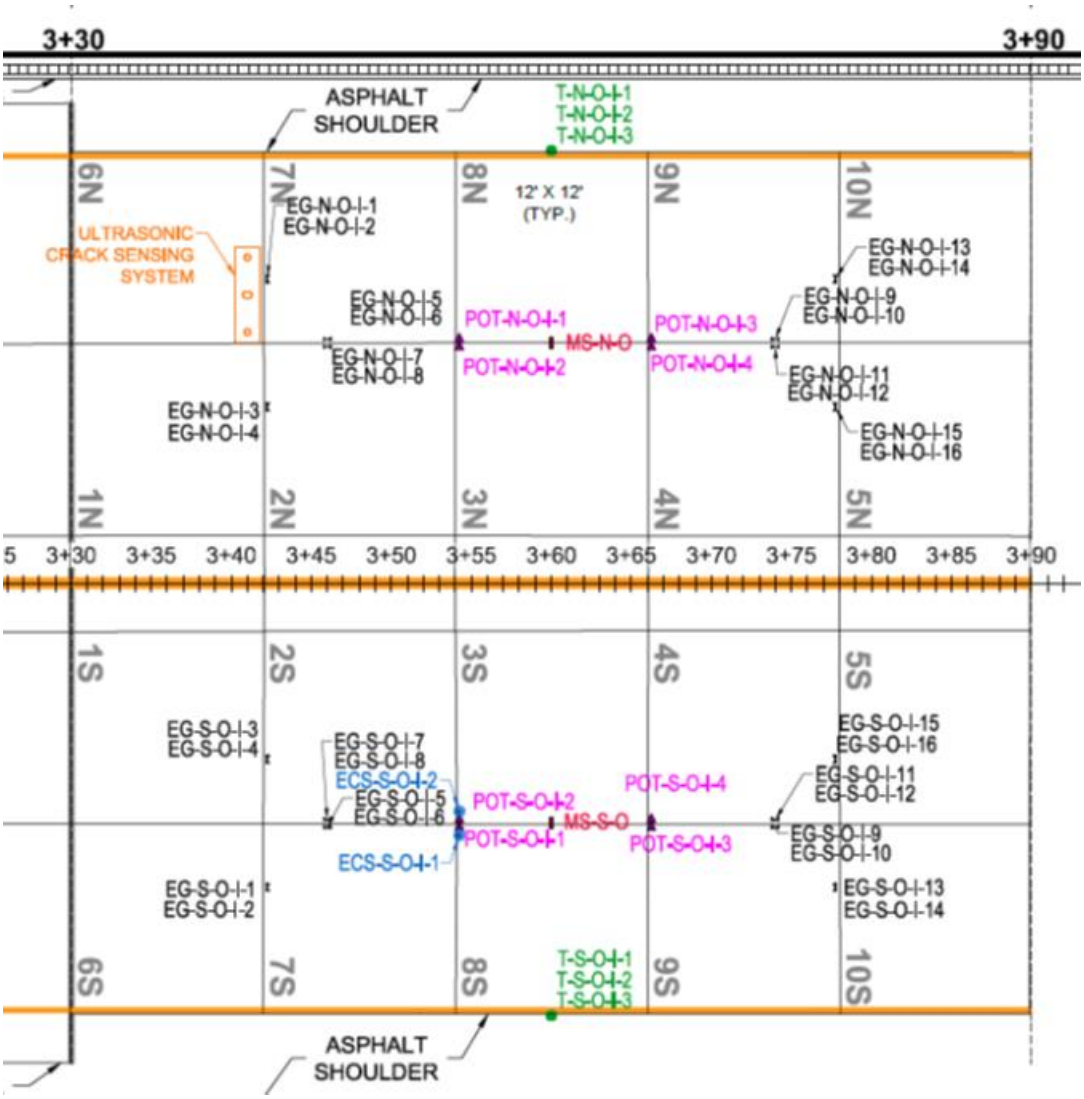

INSTRUMENT KEY		
▲	POT	POTENTIOMETER
▬	EG	EMBEDDED STRAIN GAUGE
●	T	THERMOCOUPLE
▬	MS	MOISTURE SENSOR
◉	ECS	EDDY CURRENT SENSOR
▭	UCS	ULTRASONIC CRACK SENSING SYSTEM

Figure 1. General Construction and Instrumentation Layout.

Stationing is shown in hundreds of feet.

Figure 2. Vertical Deflection-Sensing Potentiometer in Watertight Housing (Top) and Eddy Current Sensor (Bottom) Prior to Placement of Concrete Slab.

4. TEST PLAN

A test plan was developed to evaluate the effect of limited overload traffic on overall rigid pavement life. Because of the small test area available (two 24 × 60 ft. test items), the number of variables that could be considered was small. Only one of the two identical test items would receive a series of controlled overloads, based on a percentage of the computed PCN. Both test items would then be trafficked to a predefined failure condition, defined as a structural condition index (SCI) of approximately 80. The difference in applied coverages to failure will then be indicative of the effect of the initial overload. The specific steps are as follows:

1. Compute a PCN for the test pavement, using the design assumptions and the method of FAA AC 150/5335-5C (COMFAA 3.0). The PCN assumes that the design traffic is a dual (D) gear aircraft and that a reasonable number of passes to failure in this case is between 10,000 and 15,000. Test traffic will be applied using a wander pattern consisting of 66 passes on 9 discrete tracks, representing an assumed normal lateral distribution around the nominal centerline. The selected wander pattern is illustrated in figure 3.
2. Once the PCN is established, develop a series of overloads, based on dual tandem (2D) aircraft loads, with ACNs between 5% and 25% above the declared PCN.
3. After conducting initial baseline measurements of pavement properties and verifying the responses of in-pavement sensors, run one complete wander pattern (see step 1) on both test items. Check strain responses under the wheel path and compare with the thickness design.
4. On the south test item only, apply overload passes using the same wander pattern as in step 3, but using a 2D gear configuration with accordingly increased wheel loads. Apply overloads in increasing increments until either (a) observation of a crack visually or by strain gage analysis, or (b) completion of a full wander pattern at the 25% overload level.

5. Traffic both test items normally until failure is observed on one of the test items. Continue trafficking the other (non-failed) test item until both test items are at the same condition, as measured by the structural condition index (SCI).

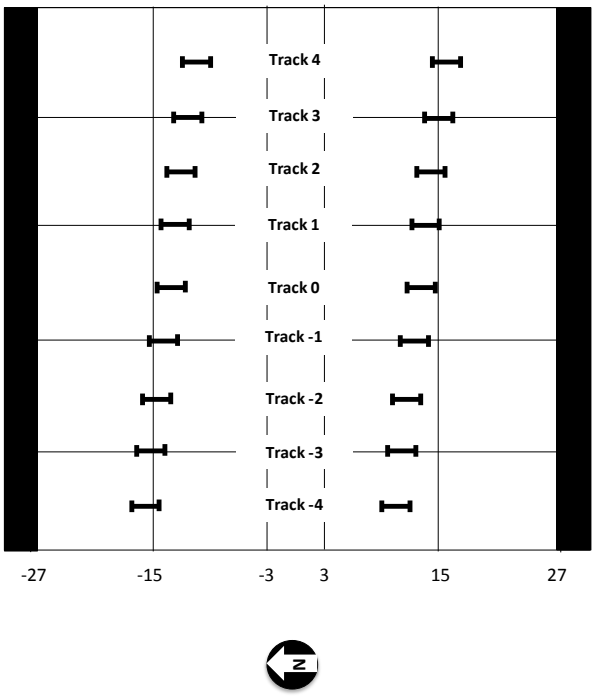

Track #	Carriage Centerline Location, ft	
	North	South
-4	-15.662	8.838
-3	-14.809	9.691
-2	-13.956	10.544
-1	-13.103	11.397
0	-12.250	12.250
1	-11.397	13.103
2	-10.544	13.956
3	-9.691	14.809
4	-8.838	15.662

Figure 3. Wander Pattern.

A key element of this test plan is continual pavement condition monitoring. This is important because the follow-on experiment in CC8, involving PCC-on-rigid overlays, will require a specific value of SCI as a starting point for the pavement receiving the overlay (Yin 2013). It is important the overload test traffic not impart too much damage. Throughout the traffic testing, the structural performance of test pavement was monitored and quantified by means of the SCI. SCI is a modification of the Pavement Condition Index (PCI) for Airports (rigid) method following ASTM D 5340 (ASTM 2012). Like PCI, SCI is based on visual inspection of the pavement surface and identification of standard distresses. The difference is that in the SCI only distresses related to structural loading are counted, while environmental and construction/material-related distresses are disregarded. In the field, pavements are divided into "sample units," and a subset of sample units is then randomly selected for inspection. Due to the small size of test area, south and north test item were considered to constitute a separate sample unit, and 100% inspection (i.e., of 10 slabs) was performed.

An evaluation of the test pavement was performed using FAARFIELD 1.4, assuming the following structure: 9 in. PCC, FAA Item P-501; 11 in. aggregate base, FAA Item P-154, average subgrade k = 120 pci. Concrete strength was taken as R = 650 psi, based on the average flexural strength (ASTM C78) of concrete beams cast at the time of construction and tested at the start of traffic. Assuming that the design traffic load is a dual (D) aircraft gear with 20,000 lbs. per wheel (corresponding to an aircraft gross weight of 84,211 lbs.), FAARFIELD predicts total lifetime traffic of 10,405 passes. This life prediction is based on the FAARFIELD 1.4 rigid

pavement failure model and a computed maximum edge stress (with assumed load transfer) of 445 psi.

The PCN was determined using the program COMFAA 3.0 and the method of AC 150/5335-5C. Assuming an improved top-of-base *k*-value (210 pci) based on the contribution of the 11 in. P-154 layer, for the above lifetime traffic, COMFAA gives a PCN value of 21.1 on a "C" subgrade. The computed ACN for the NAPTF dual gear at 20,000 lbs. per wheel and 220 psi tire pressure is 20.4 on "C" subgrade, which is less than the PCN, as expected. Therefore, the PCN was established as 21/R/C, and an initial schedule of overloads based on this PCN was established in table 1. ACNs were determined for the NAPTF 2D gear using the COMFAA 3.0 program. Note that actual percent increases over the declared PCN differ from the whole numbers, because it is only possible to control the target wheel load to increments of 500 lbs.

Table 1. Schedule of Initial Overloads.

Overload (nominal)	Overload (actual)	ACN	2D Wheel Load, lbs.
5%	4.0%	21.8	21,500
10%	10.1%	23.1	22,500
15%	13.2%	23.8	23,000
20%	19.6%	25.1	24,000
25%	26.0%	26.5	25,000

5. TRAFFIC TESTING

The traffic testing occurred in a number of stages using the NAPTF test vehicle. The dates, test vehicle configurations, wheel loads, and loading passes for each stage of trafficking are summarized in table 2.

Table 2. Traffic Testing History.

Dates (all 2016)	Traffic Type	Wheel Load, lbs.	Wanders (North)	Wanders (South)	Cumulative Passes
22 Feb	Normal I	20,000	1	1	66
22 Feb	Overload I	21,500	0	1	132
	Overload I	22,500	0	1	198
	Overload I	23,000	0	1	264
	Overload I	24,000	0	1	330
	Overload I	25,000	0	1	396
23-24 Feb	Normal I	20,000	19	19	1650
25 Feb	Normal II	28,000	1	1	1716
25-26 Feb	Overload II	28,500	0	1	1782
	Overload II	29,500	0	1	1848
	Overload II	30,500	0	1	1914
	Overload II	31,500	0	1	1980
	Overload II	32,500	0	1	2046

26 Feb - 2 Mar	Normal II	28,000	36	36	4422
9-15 Mar	Normal II	28,000	33	0	6600
14-19 Sep	Normal II	28,000	28	0	8448

Traffic testing began on February 22, 2016, following the test plan. An initial set of 66 passes of a D gear at the 20,000 lbs.-per-wheel design load was run, constituting one complete wander pattern. Following this initial wander pattern (see figure 3), five overload wander patterns (330 passes total) of incrementally increasing 2D gear loads were applied following table 1. No cracks were observed, either visibly on the surface, or by evidence of strain gage responses. The average peak tensile strain recorded on all longitudinal bottom strain gages for this wander was 59 microstrains, corresponding to a maximum tensile strain of 76 microstrains when extrapolated to the concrete bottom surface. The strain responses were notably uniform, with the average measured peak response varying from 55 to 65 microstrains under the 20-kip wheel load. The estimated peak load-induced stress for each pass was obtained by multiplying the average extreme fiber strain by the in-situ Portable Seismic Pavement Analyzer (PSPA) concrete modulus E = 4,300 ksi. The resulting value, 319 psi, is significantly less than the 445 psi design stress from the FAARFIELD model. This is not surprising, given that the FAARFIELD design model contains a number of conservative assumptions (fully unbonded slab-base interface, infinite subgrade depth) that may not be reflected in the built structure. Since the true load-induced peak stress is less than 50% of the reliably estimated concrete strength (650 psi), a reasonable conclusion is that the PCC slabs will not fail in fatigue at the planned load, even if a very large number of passes were to be applied.

Based on the above analysis, it was decided to increase the PCN based on the structural capacity estimated from strain gages. Assuming that the concrete stress remains proportional to the load for undamaged slabs, the dual wheel tire load P that actually will produce a tensile stress of 445 psi in the slabs, and thus fail the section in the predicted number of passes, is computed by simple linear proportion:

$$P = \frac{445}{319} \times 20{,}000 \text{ lbs.} = 27{,}900 \text{ lbs (say } 28{,}000 \text{ lbs)} \qquad (1)$$

Again using COMFAA 3.0, it was found that the ACN of the NAPTF test vehicle dual gear at a new wheel load of 28,000 lbs. and 220 psi tire pressure is 29.9. Therefore, the test pavement PCN was reassigned the value 30/R/C. New overload values for the 2D gear load are given in table 3.

Table 3. Schedule of Revised Overloads.

Overload (nominal)	Overload (actual)	ACN	2D Wheel Load, lbs.
5%	4.7%	31.4	28,500
10%	9.3%	32.8	29,500
15%	14.3%	34.3	30,500
20%	19.3%	35.8	31,500
25%	24.3%	37.3	32,500

The revised overload test was executed on February 25 and 26. A per-wheel load of 28,000 lbs. was used for normal traffic, and the values in table 3 were followed for overloads. The maximum bottom tensile strain was 72 microstrains at a wheel load of 32,500 lbs. An extreme fiber strain of 93 microstrains resulted in approximately 400 psi working stress which was still lower than the FAARFIELD calculated critical stress.

Traffic testing was stopped on March 2 after 4,422 normally loaded passes at the increased wheel load level. A number of distresses were observed on the south test item near the transverse joint at Sta. 3+54, which caused the SCI value to drop from 100 to 68. The observed distresses were:

- 1 shrinkage crack on Slab 2S
- 1 low severity diagonal crack and 1 low severity corner spall on Slab 3S
- 1 low severity corner break on Slab 7S
- 1 medium severity corner break on Slab 8S

A photograph of the damaged pavement is shown in figure 4a. Examination of the distress patterns suggested the development of cracking near the slab surface as a result of tensile stresses due to slab counter-flexural bending.

After rest period of approximately six months, traffic resumed on the north test item only (September 14). Traffic on the north test item was stopped on September 19, after completion of 7,788 normally loaded passes at a wheel load of 28,000 lbs. (1,320 passes at the original load, plus 6,468 passes at the increased wheel load). A number of distresses were found on the south test item near the transverse joint at Sta. 3+54, causing the SCI value to drop from 100 to 79. The observed distresses were:

- 1 low severity corner break on Slab 2N
- 1 low severity corner break on Slab 7N
- 1 low severity corner break on Slab 8N

A photograph of the damaged pavement is shown in figure 4b. Similar to the south test item, the distresses observed in the north test item were consistent with top-down cracking.

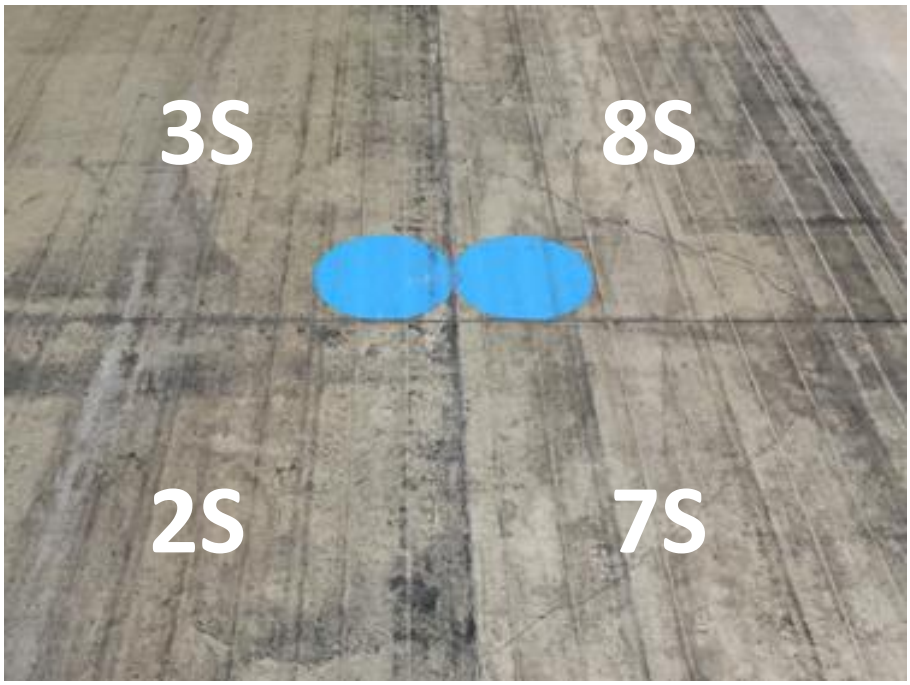

(a) South test item

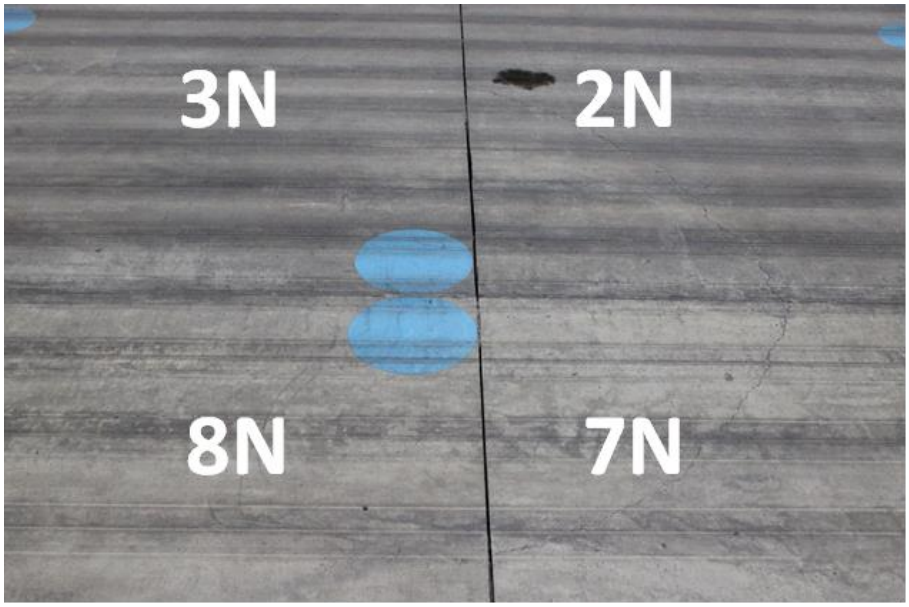

(b) North test item

Figure 4. Distresses on Pavement.

6. BEARING CAPACITY ANALYSIS

Heavy falling-weight deflectometer (HWD) testing was conducted prior to and after the traffic test. HWD test locations included all slab centers and west corners, as indicated by the blue dots in figure 5. HWD testing was conducted using a KUAB Model 150 tester with a four-drop loading sequence beginning with an approximate 12,000-lb seating load. The subsequent loads

were approximately 4,700 lbs., 8,000 lbs., and 12,000 lbs. Drop loads were kept low intentionally to avoid damaging the PCC. Raw deflection data were first normalized by adjusting deflections to a standard load (i.e., 4,700, 8,000, and 12,000 lbs).

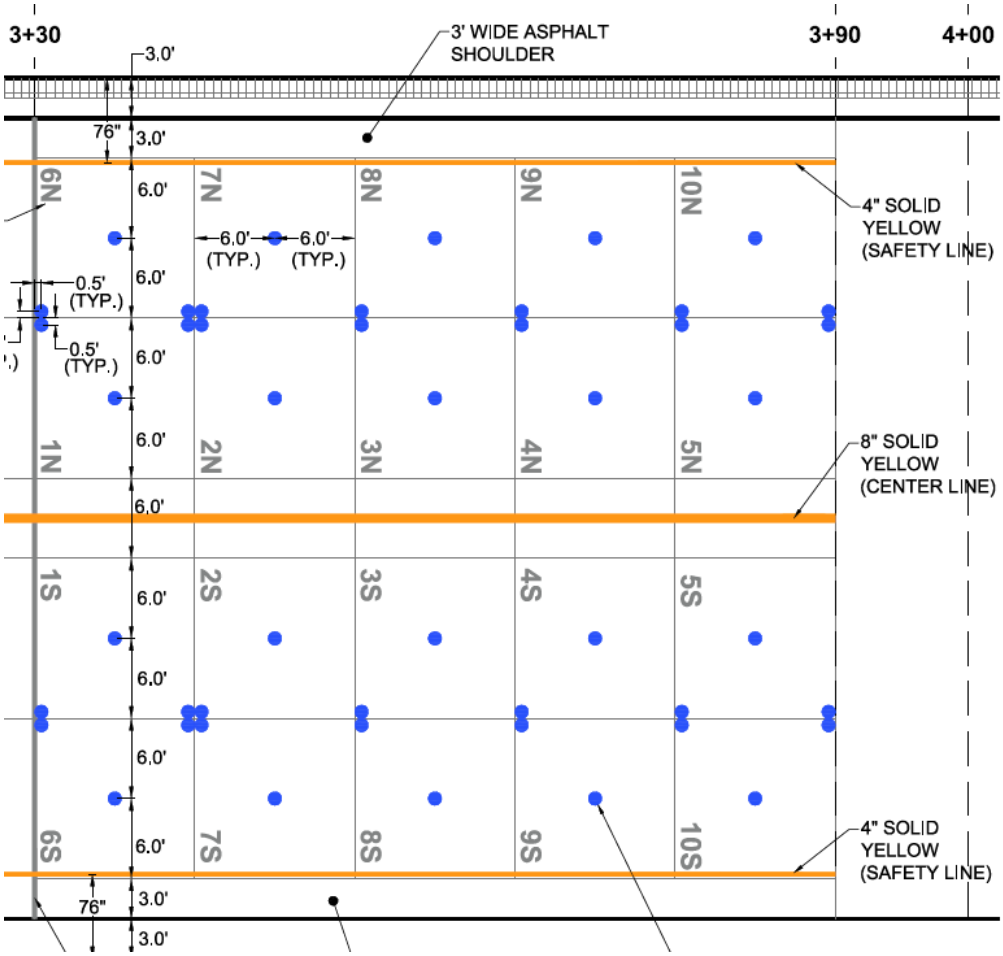

Figure 5. HWD Testing Locations.

7. SLAB CENTER DEFLECTIONS

Deflections at the highest HWD load level (12,000 lbs) are plotted in figures 6 and 7 for the south and north test item, respectively. It is clear that the pressure exerted by wheel loads distributed to the subbase and subgrade was relatively low and most of the load was carried by concrete slabs. In general, deflections increased as the traffic testing continued and the basins remained in ordinary shape through the course of trafficking. For the south test item, as shown in figure 6, it seems that the traffic induced deterioration primarily occurred at the shallow depth. For the north test item, figure 7 suggests some damage accumulated in deeper layers during trafficking. At the end of traffic testing, the deflection basins on the north test item were significantly altered.

In addition to visual examination of deflection basins, deflection basin area (*AREA*), and impulse stiffness modulus (*ISM*) were used to characterize the pavement strength. The following equations were used to calculated *AREA* and *ISM*.

$$AREA = \left[6 + 12\left(\frac{D_{12}}{D_0}\right) + 12\left(\frac{D_{24}}{D_0}\right) + 6\left(\frac{D_{36}}{D_0}\right)\right] \quad (2)$$

Where:
AREA = AREA, inches
D_0 = Maximum deflection at the center of the load plate, mils
D_{12} = Deflection at 12 in from the load plate center, mils
D_{24} = Deflection at 24 in from the load plate center, mils
D_{36} = Deflection at 36 in from the load plate center, mils

$$ISM = \frac{P}{D_0} \quad (3)$$

Where:
ISM = Impulse Stiffness Modulus, kips/inch
P = Applied load, kips
D_0 = Maximum deflection at the center of the load plate, mils

As depicted in figures 8 and 9, both AREA and ISM implied a uniform pavement structure prior to traffic testing. However, neither AREA nor ISM provides consistent indication of the decrease of bearing capacity due to traffic loads. In other words, the strength reduction (increase of AREA) was noticeable on the north test item while the stiffness reduction after the traffic testing was more pronounced on the south test item.

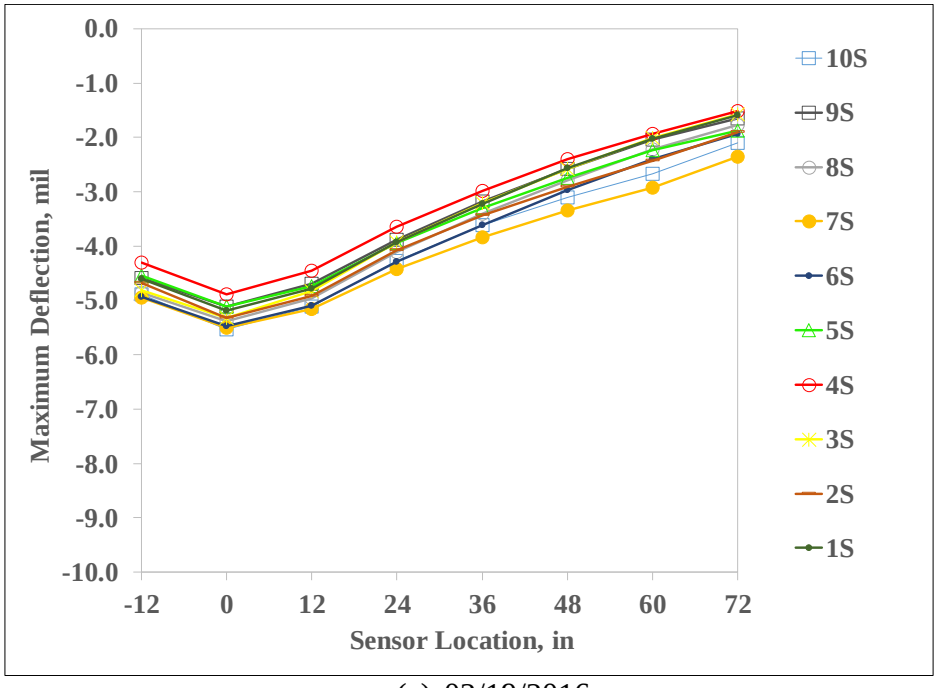

(a) 02/19/2016

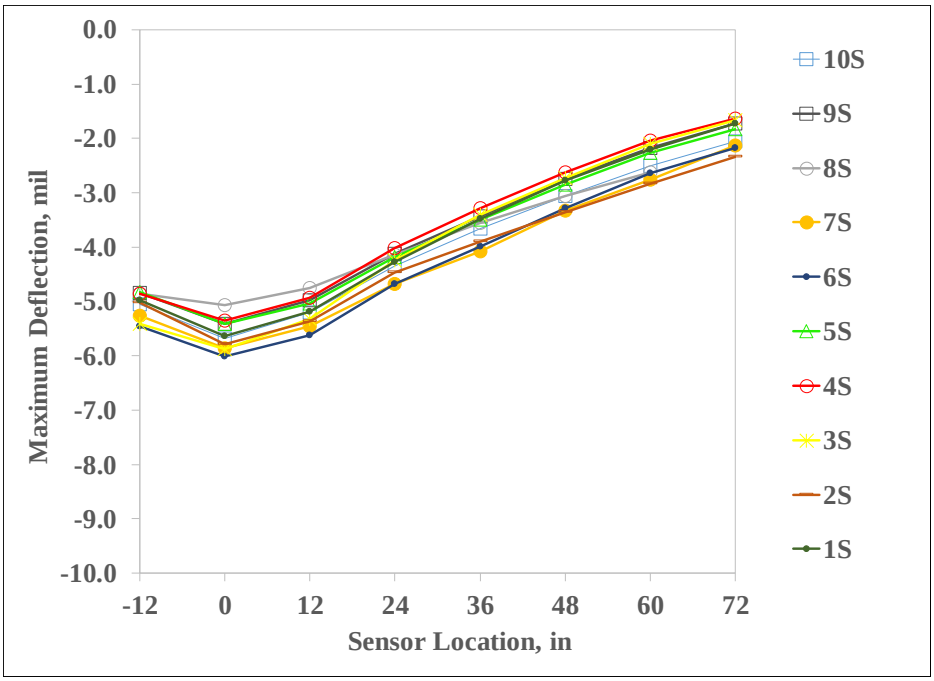

(b) 03/03/2016

Figure 6. Slab Center Deflections, South Test Item.

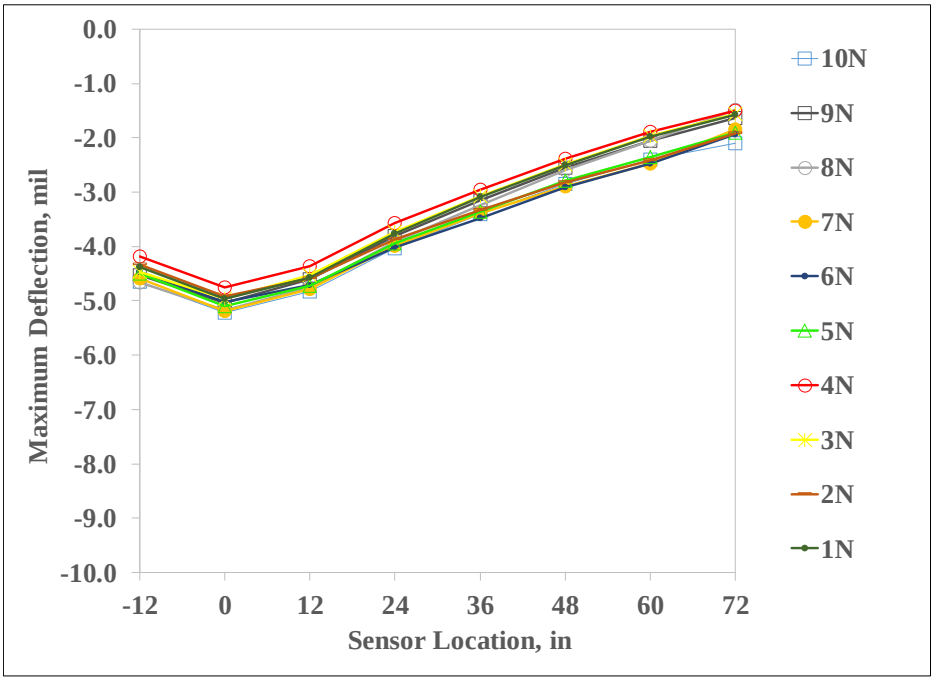

(a) 02/19/2016

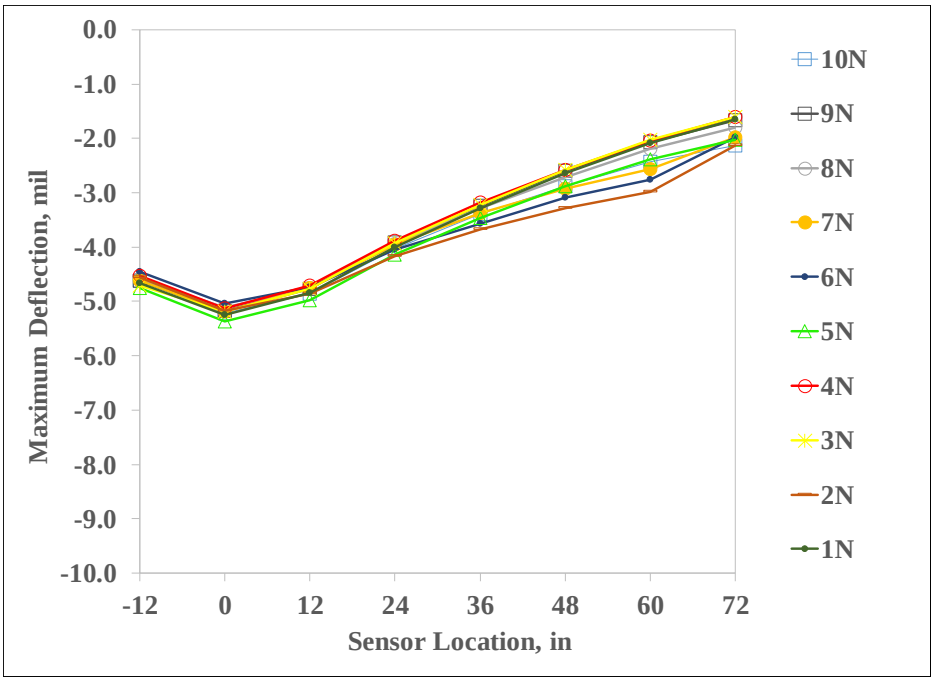

(b) 03/03/2016

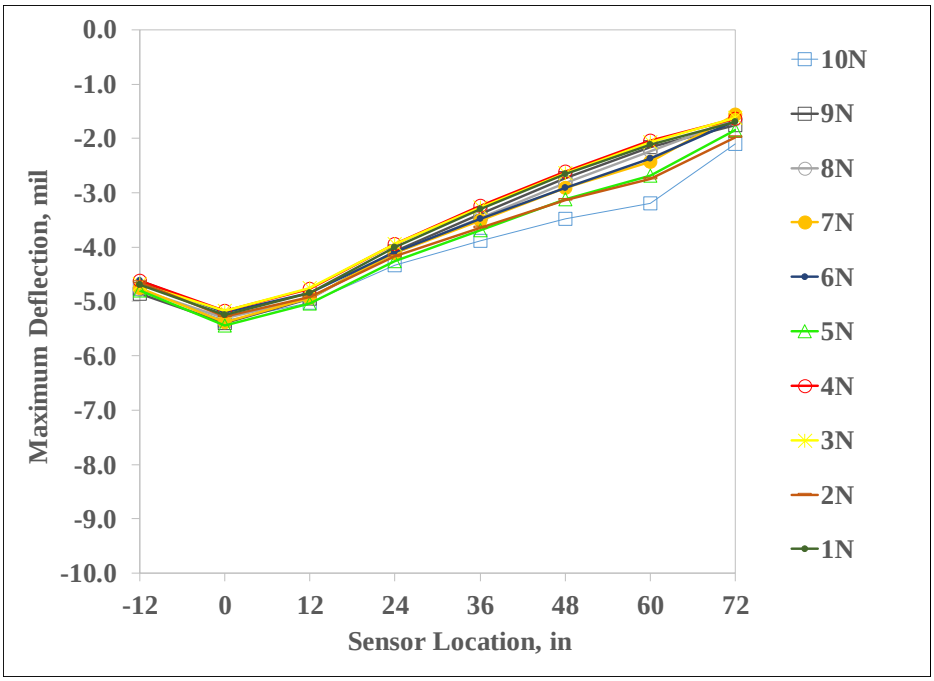

(c) 09/12/2016

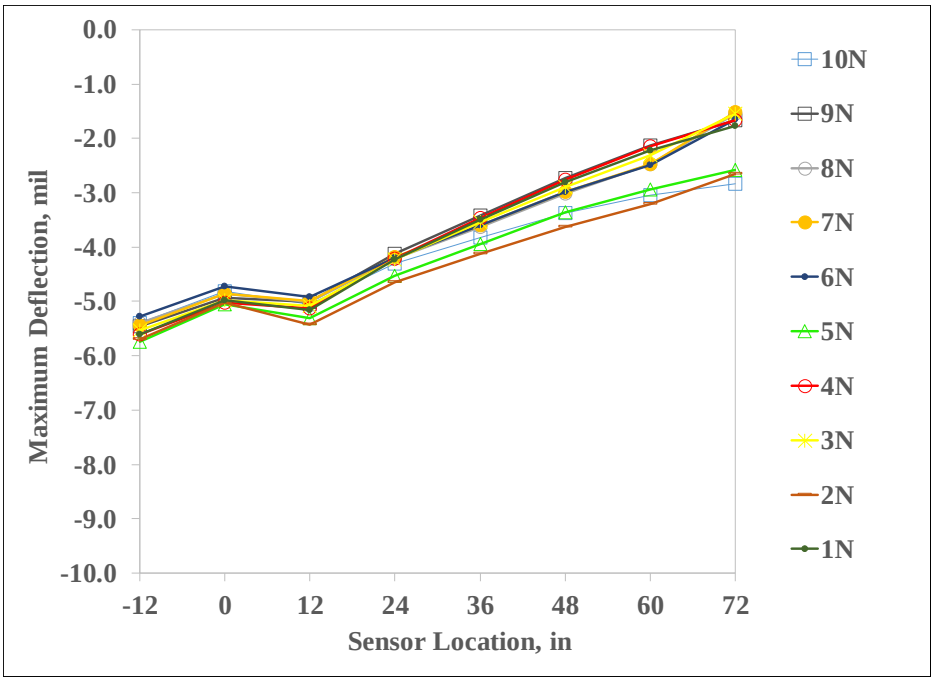

(d) 09/22/2016

Figure 7. Slab Center Deflections, North Test Item.

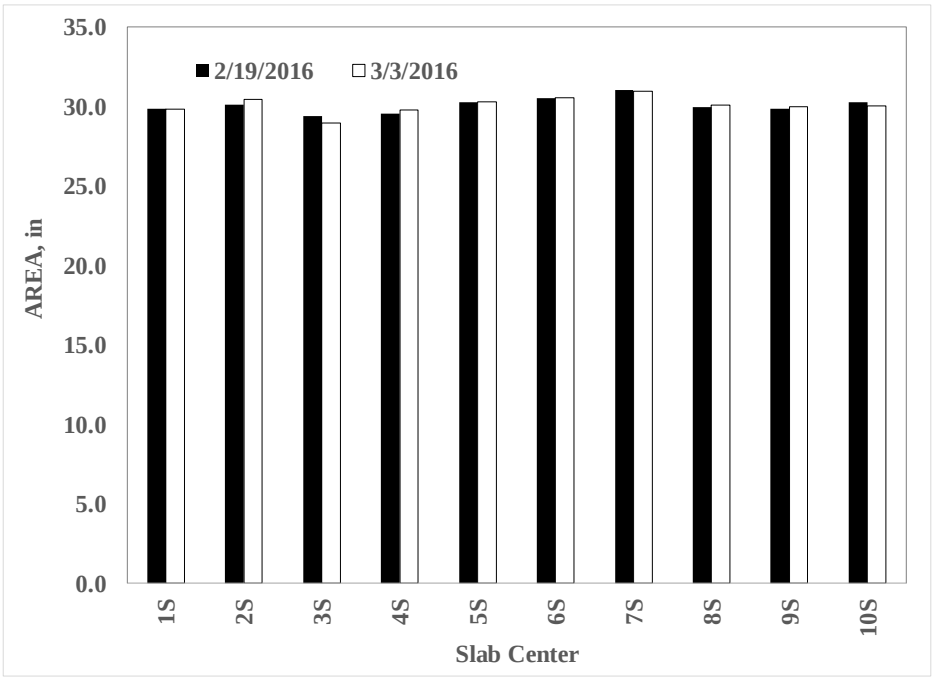

(a) South test item

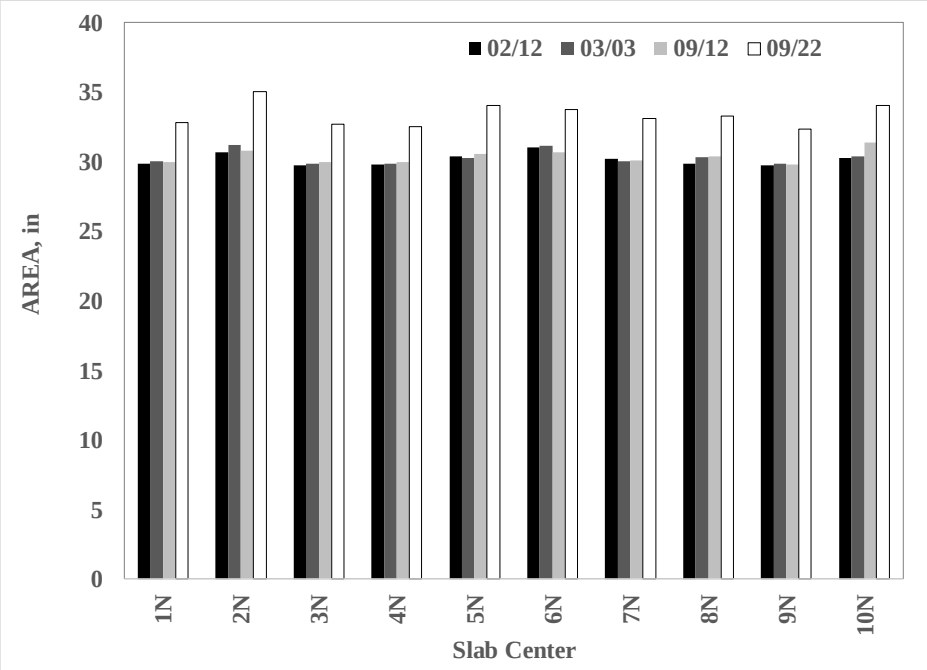

(b) North test item

Figure 8. AREA.

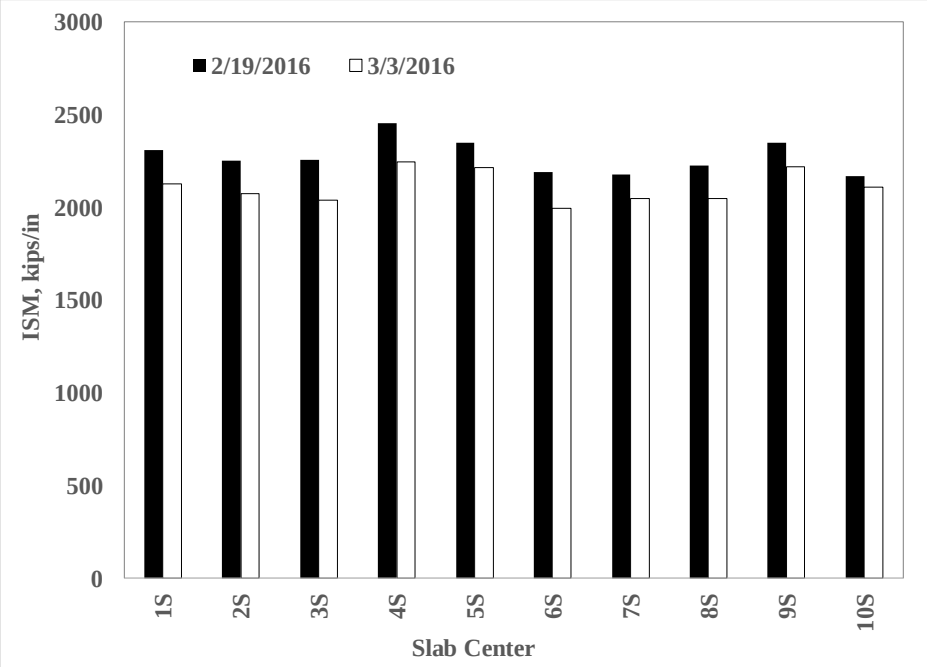

(a) South test item

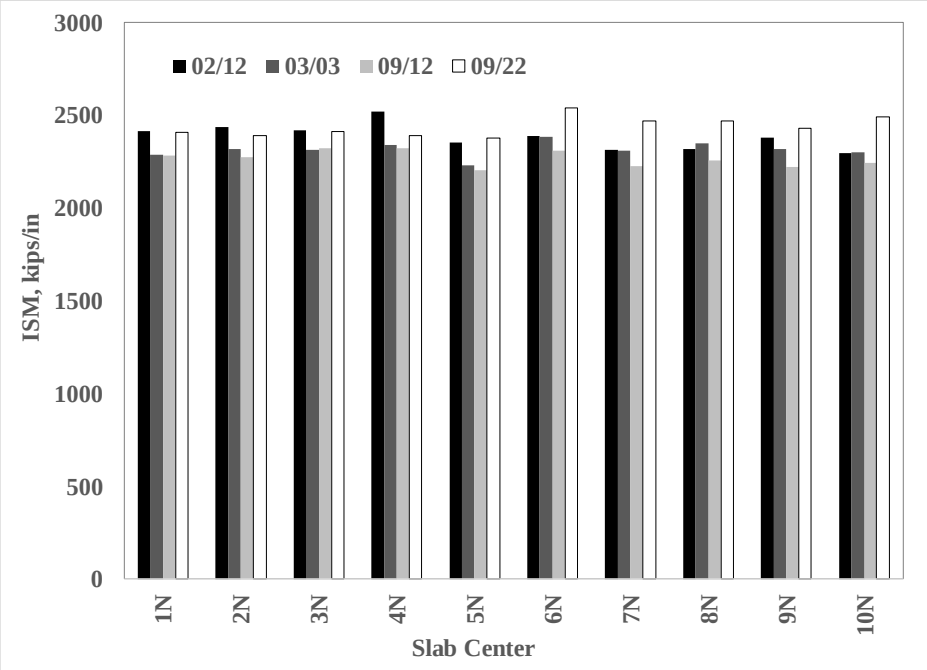

(b) North test item

Figure 9. Impulse Stiffness Modulus.

8. SLAB CORNER DEFLECTIONS

Corner HWD deflections at the highest HWD load level (12,000 lbs) were analyzed to evaluate the impact of traffic loads on slab corners. HWD testing was not conducted at the northwest corner of slab 2N and the southwest corner of slab 7N to avoid possibly damaging the experimental crack sensing system at that location. Figures 10 and 11 show pre- and post-traffic corner deflections for the remaining slabs. The south test items showed little evidence of corner deterioration based on HWD. Two factors may have contributed to the high deflections observed at the west corners of Slab 3S, 8S, 3N, and 8N. One possibility is weak support and imperfect contact with the subbase due to inadequate subbase compaction prior to concrete placement. However, from construction records there is no evidence that poor compaction was an issue. A more likely explanation is significantly reduced load transfer due to complete formation of the transverse joint at Sta. 3+54. As previously noted, all transverse joints in the overload test area are undoweled and were initiated by a saw-cut. Load transfer, if it exists, must be developed in vertical shear through the crack face roughness (aggregate interlock). The much smaller deflections (D1, -12 in) on the unloaded slabs imply that the transverse joint at Sta. 3+54 was formed at some point prior to trafficking, presumably due to temperature-induced contraction. The post-traffic deflection basins at the same four slab corners indicate severe damage in the concrete slabs that were not able to effectively transfer the loads to underlying layers. Based on the data in figures 10b and 11d, it may be surmised that the shrinkage crack observed on Slab 3S and the corner break on Slab 8S were not yet full-depth at the time of completion of traffic testing, while the corner break observed on Slab 8N most likely had progressed already to the bottom of the slab.

9. VOID DETECTION

One important characteristic of concrete pavements is the slab support conditions. The occurrence of surface distresses such as corner breaks, joint faulting, and slab cracking, can be resulted from a loss of support. Figures 12 and 13 show the maximum corner deflections (D_0) from three HWD load levels for the south and north test item, respectively. Because the pre-traffic deflections (figures 12a and 13a) pass through the X-axis near the origin, good support existed beneath the slab corners. By the completion of traffic testing (figure 12b and 13d), a deflection intercept greater than 5 mils was observed at the corners of Slab 3S, 8S, and 8N, which indicates a severe loss of support. One possible explanation of the presence of a void was the settlement under the P-501 layer as a result of traffic testing. When the traffic testing resumed in September, the voids under the corners of Slab 3N and 8N became less noticeable due to the recovery of unbound materials during non-traffic period (figures 13b and 13c).

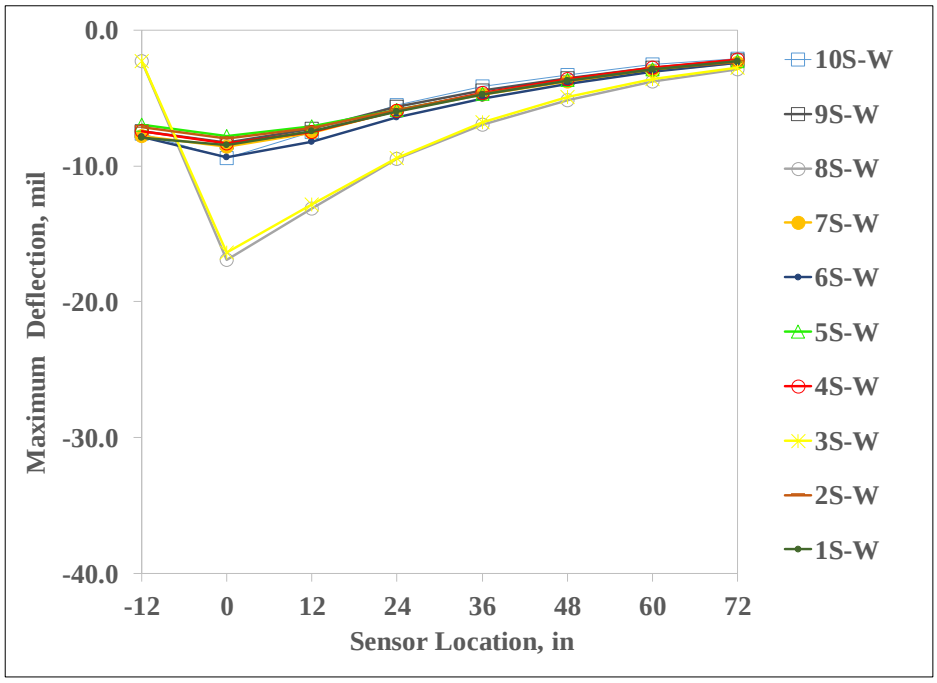

(a) 02/19/2016

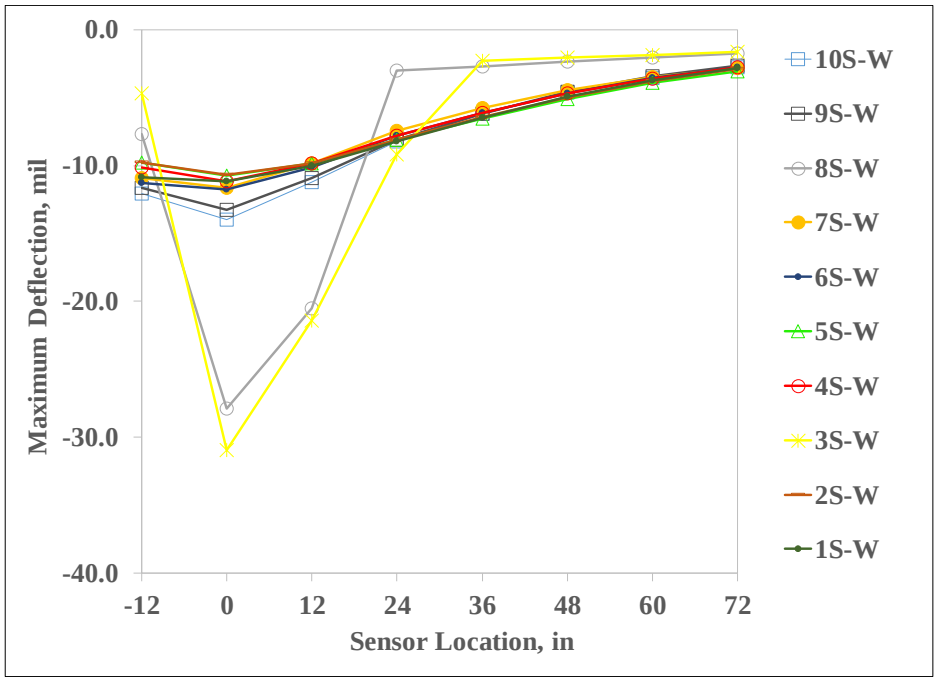

(b) 03/03/2016

Figure 10. Slab Corner Deflections, South Test Item.

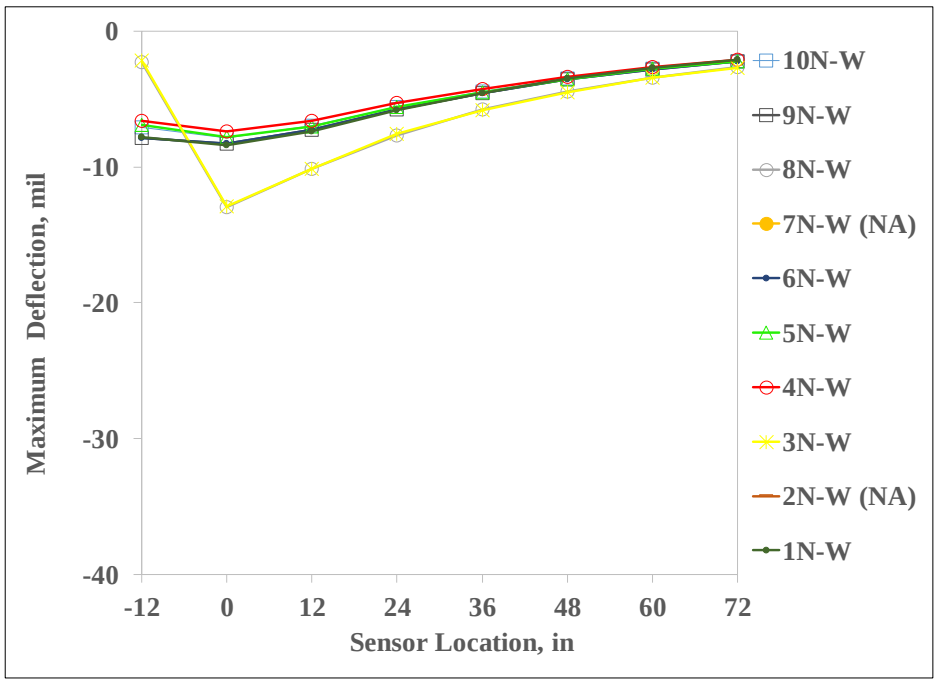

(a) 02/19/2016

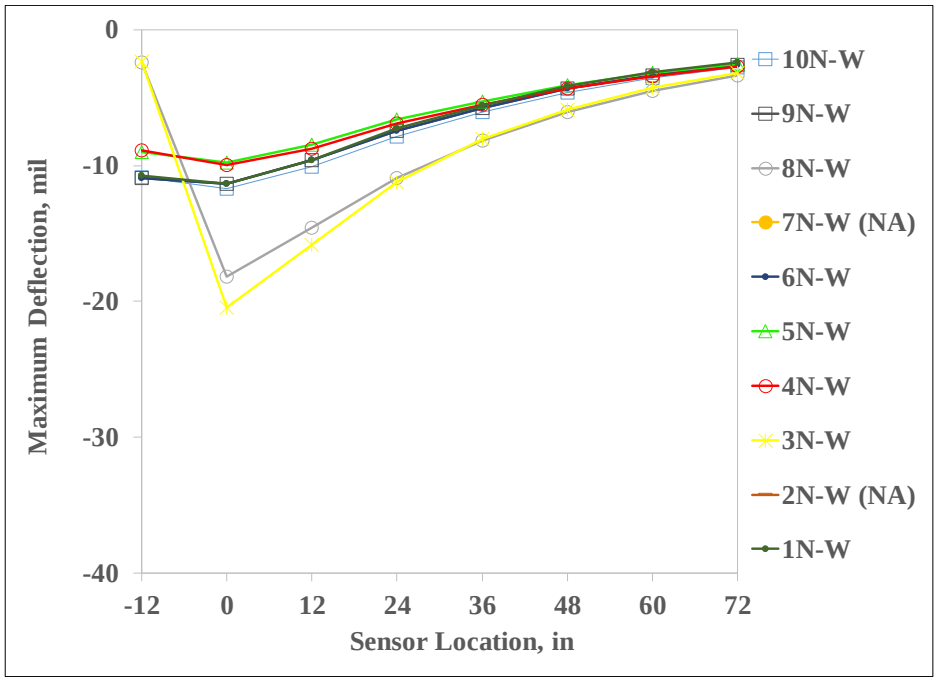

(b) 03/03/2016

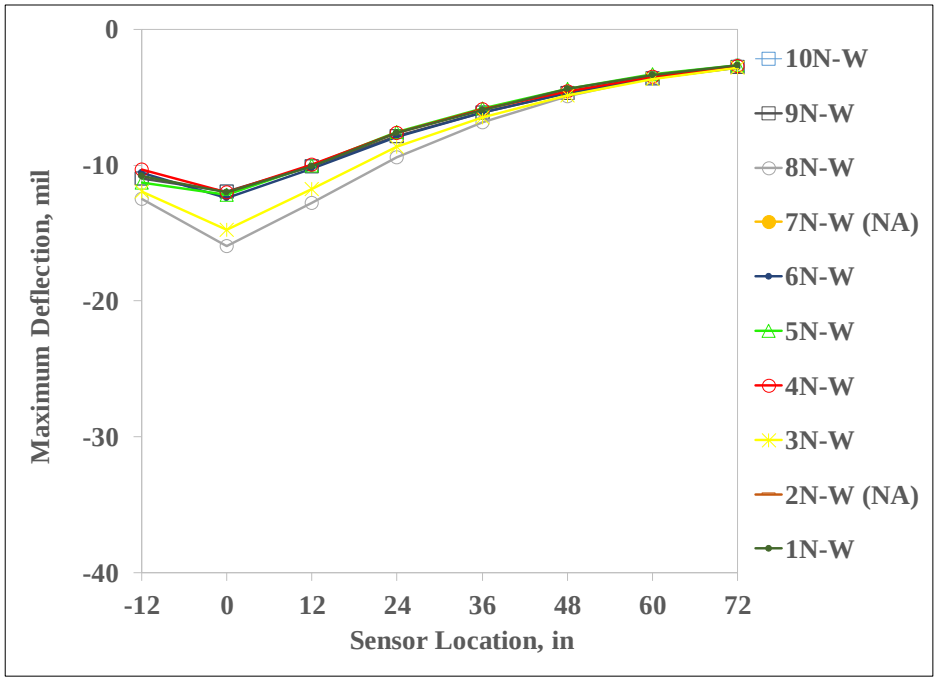

(c) 09/12/2016

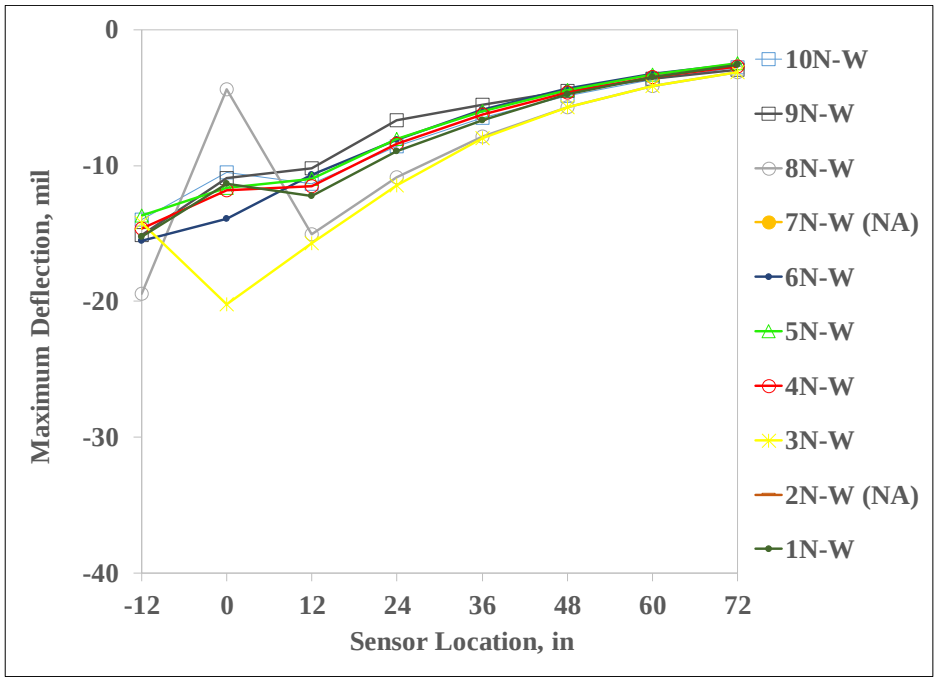

(d) 09/22/2016

Figure 11. Slab Corner Deflections, North Test Item.

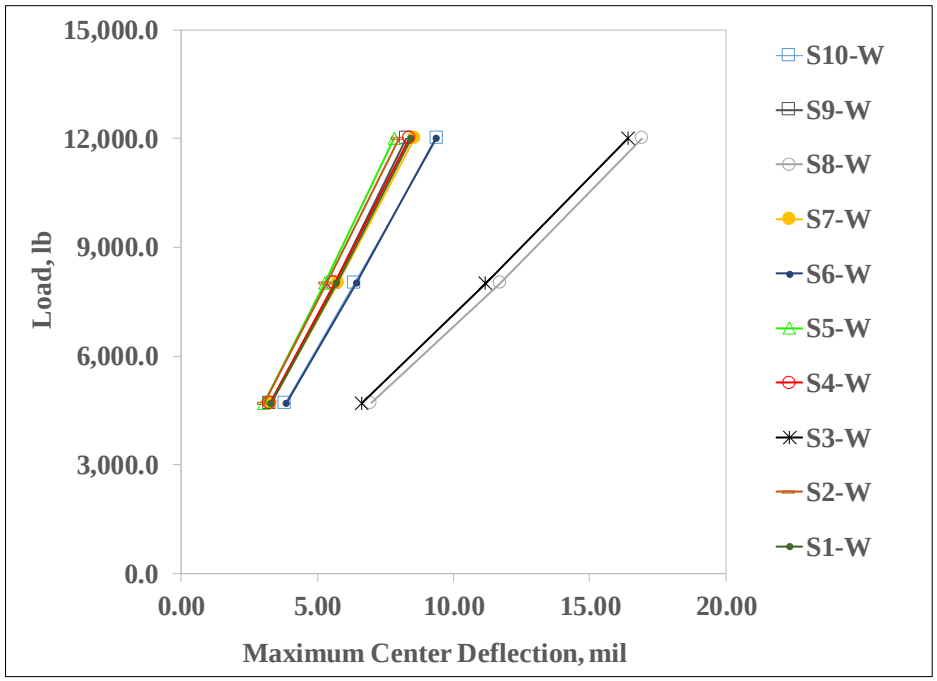

(a) 02/19/2016

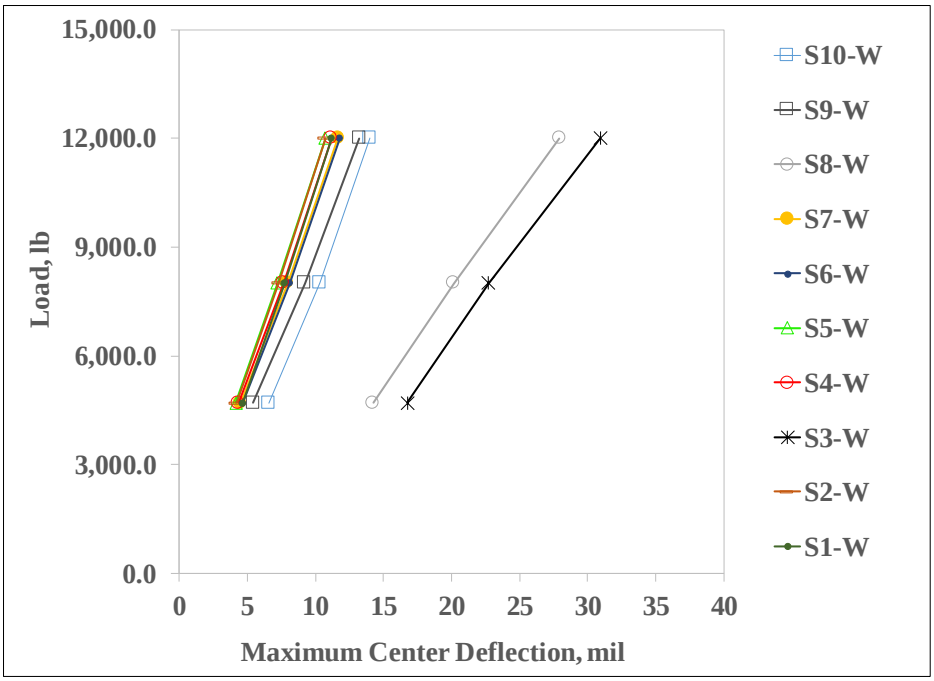

(b) 03/03/2016

Figure 12. Void Detection, South Test Item.

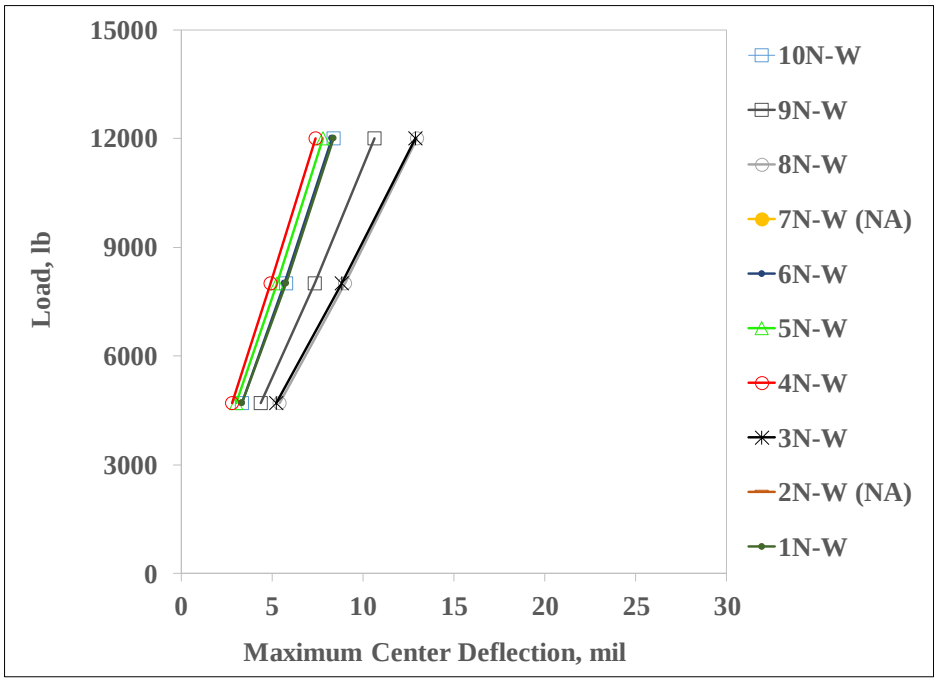

(a) 02/19/2016

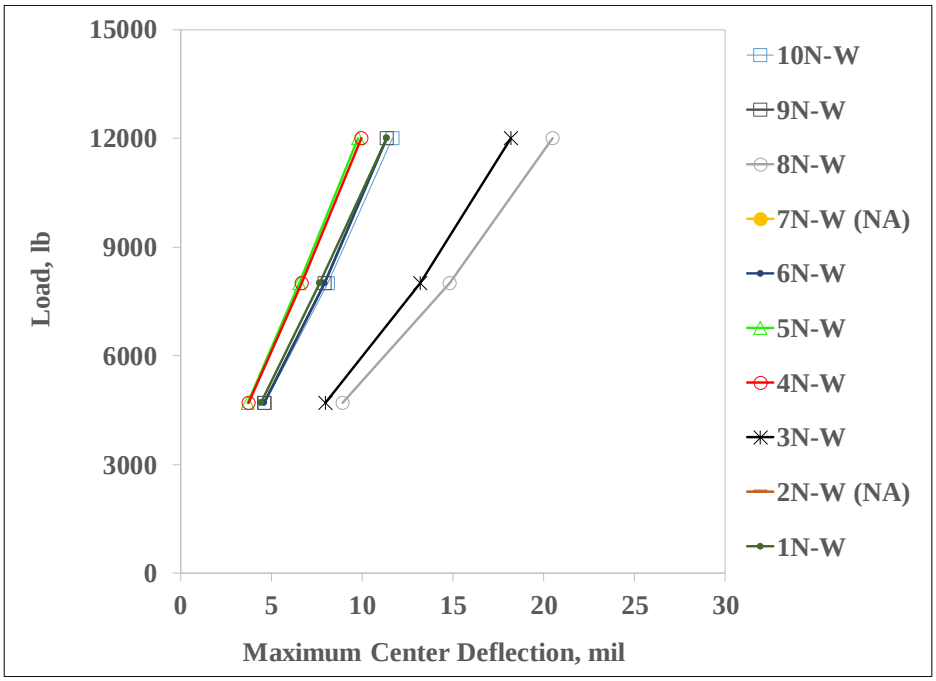

(b) 03/03/2016

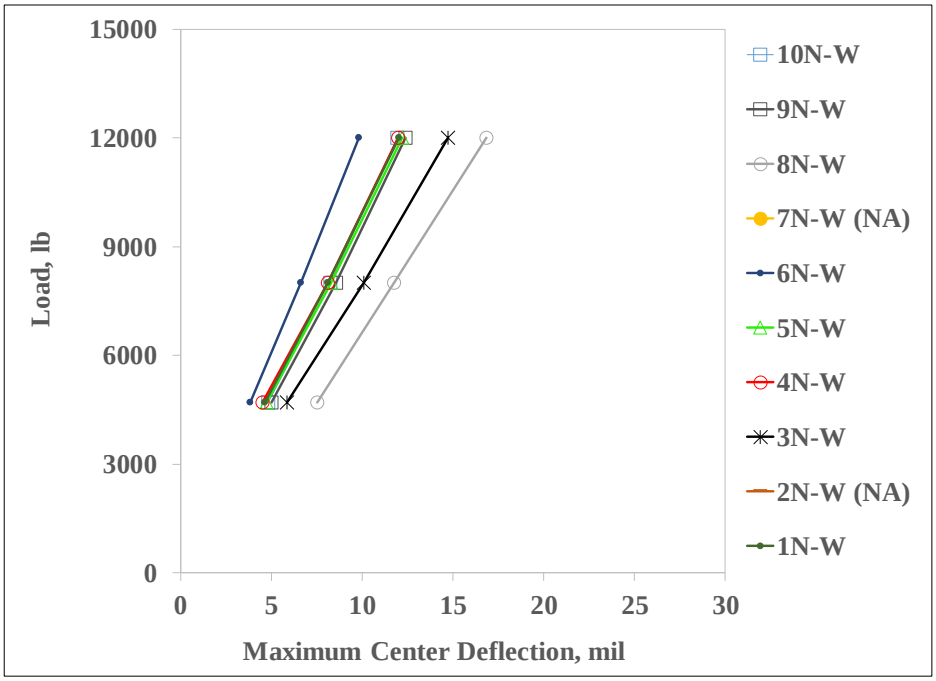

(c) 09/12/2016

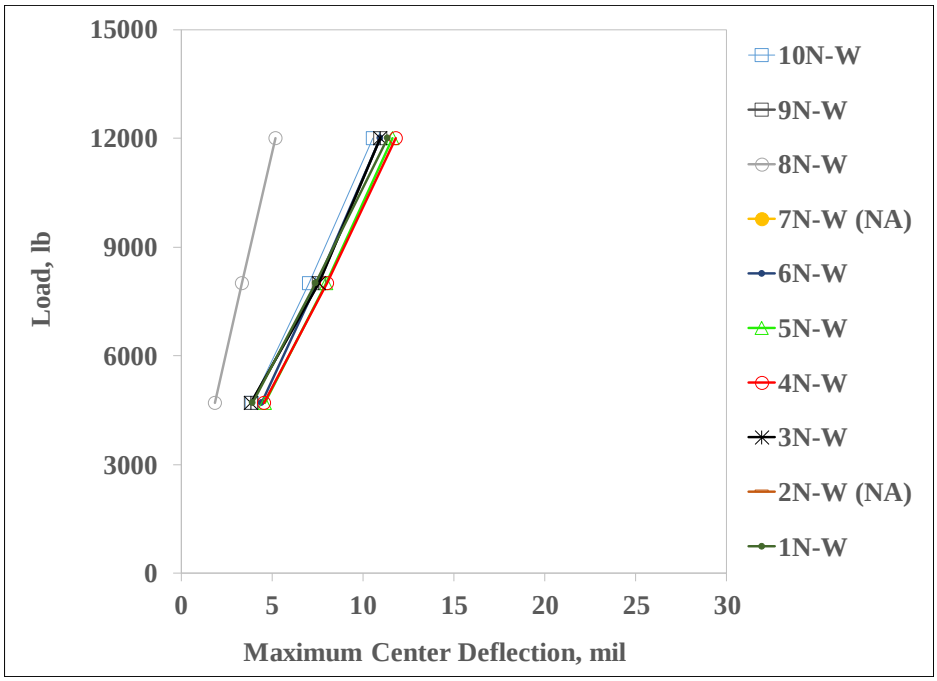

(d) 09/22/2016

Figure 13. Void Detection, North Test Item.

Past NAPTF studies have shown that indoor concrete slabs may be susceptible to corner uplift driven by moisture gradients. Therefore, prior to the traffic test, the slabs were watered twice a week in order to minimize moisture gradients. Watering increased the humidity in the top surface and thereby reduced the negative moisture gradient and minimizes upward curling. As shown in figures 12 and 13, a fairly linear pattern of deflections at different load levels suggests the occurrence of trivial curling.

10. IN-SITU LAYER MODULI ANALYSIS

For each individual slab, the FAA's BAKFAA program was used to backcalculate the layer elastic moduli using the slab center deflection basins under the heaviest HWD load. BAKFAA uses the layered elastic analysis program LEAF to compute the layer moduli based on the deflection basin data, layer thicknesses, and the composition of the pavements, and minimizes the sum of the squares of difference between the measured and computed vertical deflections in order to find the best-fit set of moduli. The initial set of layer elastic moduli (seed values) and Poisson's ratios are provided in table 4. While the pre-traffic seismic modulus was used as the seed value for the concrete (E_c), the initial subgrade elastic modulus ($E_{subgrade}$) was estimated from the plate load test k value using the following equation:

$$E_{subgrade} = 20.15k^{1.284} \quad (4)$$

The seed modulus of subbase ($E_{subbase}$) and Poisson's Ratio of each layer were selected from tables 13 and 14 in the Advisory Circular (AC) 150/5370-11A (FAA 2011). As for the layer

interface bonding conditions, all interfaces were treated bonded except for the concrete layer. The as-built thickness of each pavement layer was used.

Table 4. BAKFAA Inputs.

Layer	Seed Modulus, ksi	Poisson's Ratio	Interface Parameter	Layer Changeable
Concrete	E_c (3635-5050)	0.15	0	Yes
Subbase	$E_{subbase}$ (50)	0.30	1	Yes
Subgrade	$E_{subgrade}$ (13.6)	0.40	1	Yes

The load induced-stresses and strains in most pavement structures dissipate to almost zero value within a few feet from the pavement surface due to the arching effects in the soil. Hence, such stresses cause no measurable deflection. To improve the convergence of stresses and deflections at deeper locations, the BAKFAA allows the placement of a stiff layer (depth to bedrock) at a certain depth below the pavement surface. In this study, the need of including a stiff layer in the backcalculation was evaluated using the equivalent (or composite) modulus of the pavement (AASHTO 1993):

$$E = \frac{P(1-\upsilon^2)}{\pi(r)(d_r)} \quad (5)$$

Where:
E = Equivalent modulus, psi
P = Applied load (12000 lb)
υ = Poisson's ratio (0.40)
d_r= Deflection measured at r distance from the center of the load, inches
r = Radial distance from the center of load to the deflection sensor in question, inches

A plot of the calculated equivalent modulus versus the radial distance is given in in figure 14. The E value at the curve tail is nearly constant with increasing distance. This trend implies a relatively deep stiff layer. Therefore, a depth to bedrock of 10 feet from the pavement surface was introduced in the BAKFAA.

Prior to and after the traffic testing, the portable seismic pavement analyzer (PSPA) was used to measure the seismic modulus of P-501 layer. At each slab center and selected slab corners (figure 2), multiple PSPA measurements were collected at different orientations, and the average values were reported. As shown in figure 15, a good agreement between the backcalculated elastic moduli and the measured seismic modulus for the P-501 layer was observed. pre-traffic seismic modulus was quite consistent from one slab center to another with an average of 4325 ksi. This average was only slightly higher than the mean value of concrete modulus from static modulus test (ASTM C649) on cylinders tested at 40 days (4211 ksi). Nazarian et. al (2006) reported that PSPA could overestimate the concrete modulus from the laboratory cylinder test.

Using Equation 6, the averaged backcalculated E_c yielded a concrete modulus of rupture of 671 psi, which is 5% higher than the laboratory measured flexural strength of field cured beams (172 days), 638 psi.

$$M_R = 43.5\left(\frac{E_c}{10^6}\right) + 488.5 \quad (6)$$

The pavement deterioration due to traffic loading was then evaluated by comparing the layer moduli over time. Figures 16 and 17 suggest that pavement deterioration (modulus reduction) occurred in the P-501 layer, about 10% for the south and 20% for the north test item, respectively.

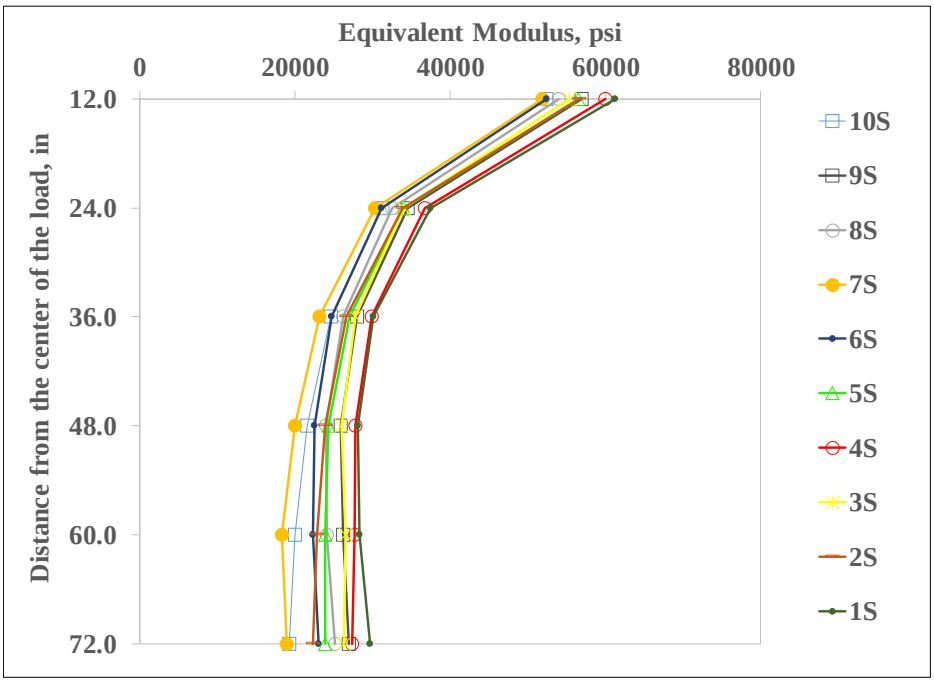

(a) South

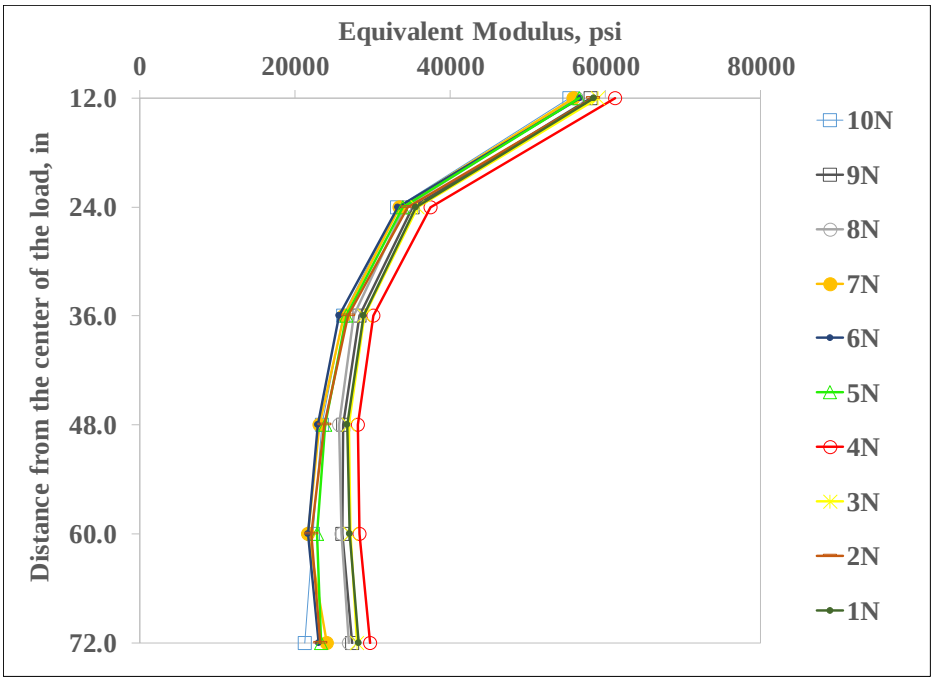

(b) North

Figure 14. Equivalent Pavement Modulus vs. the Distance from the Center of Load.

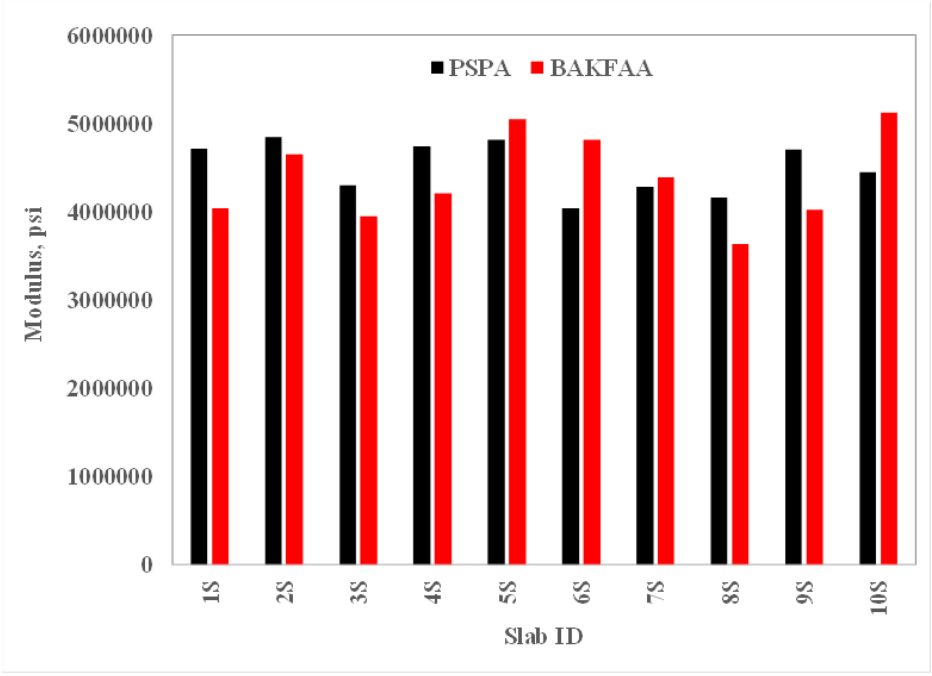

(a) South

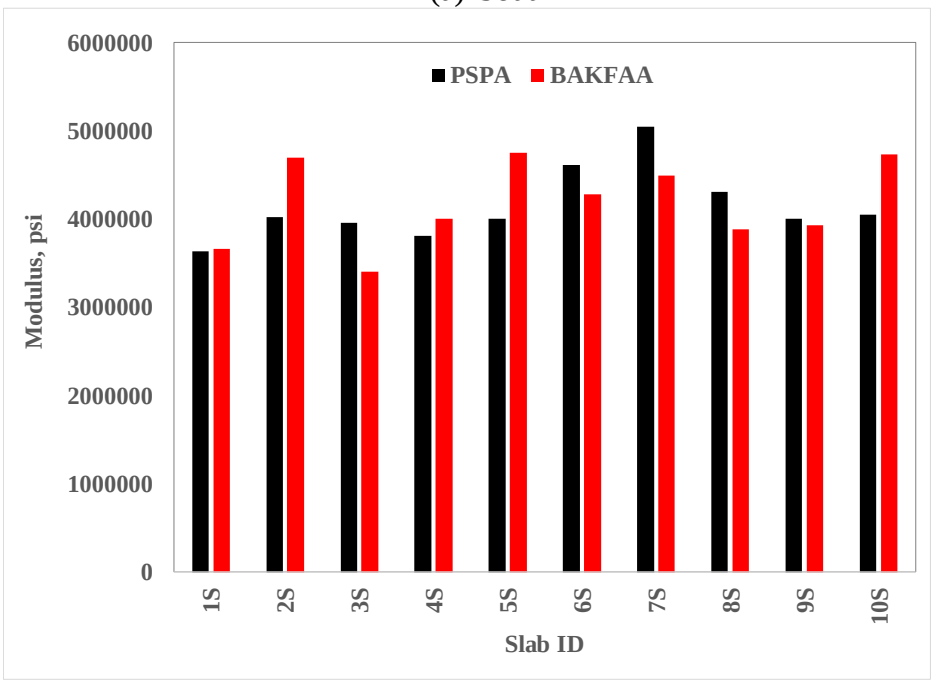

(b) North

Figure 15. Comparison of Pre-Test Backcalculated and PSPA Concrete Modulus.

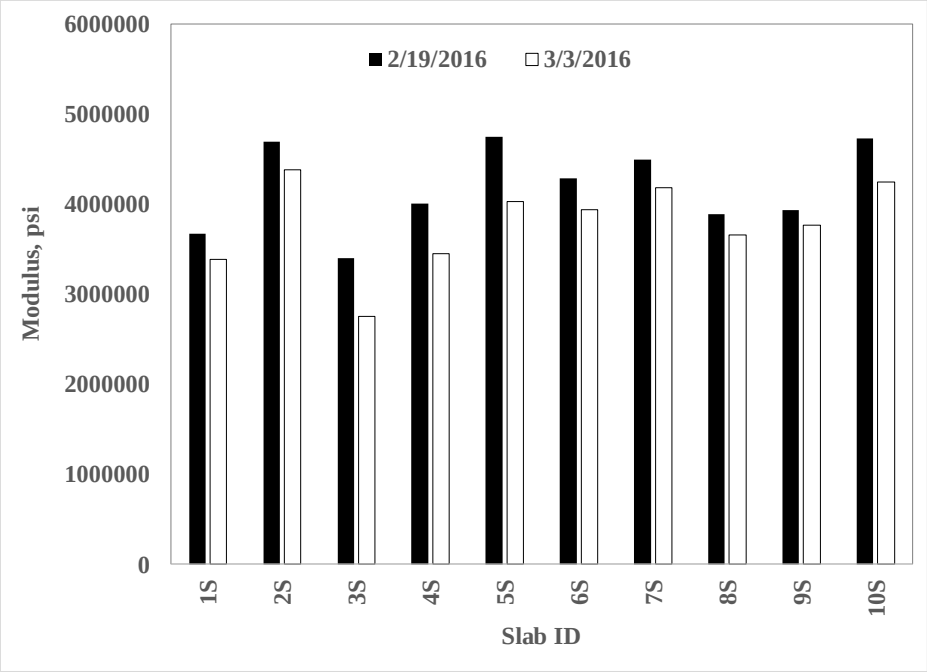

(a) Concrete

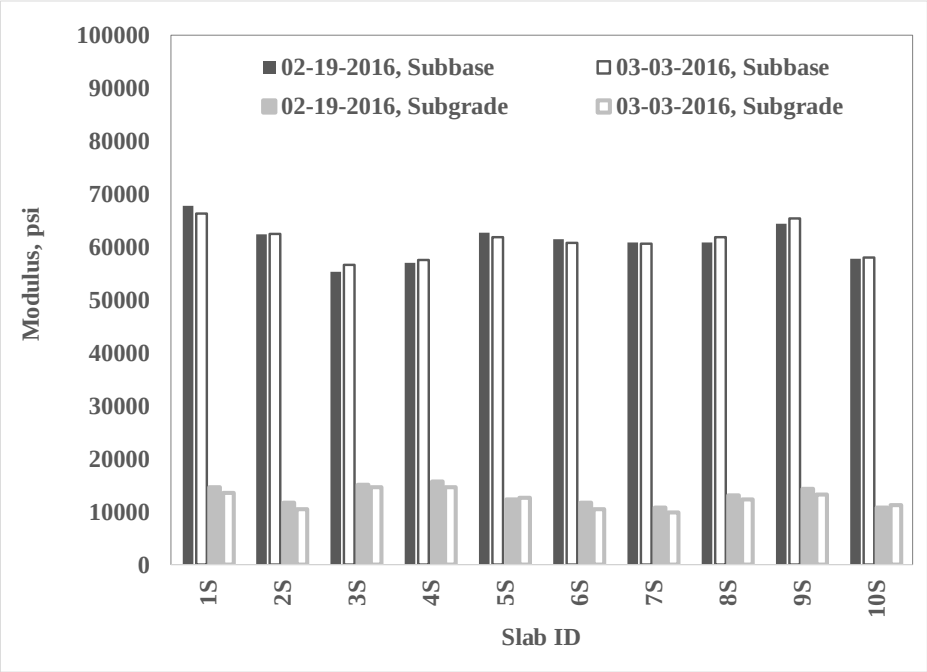

(b) Subbase and subgrade

Figure 16. Backcalculated Layer Moduli over Time, North Test Item.

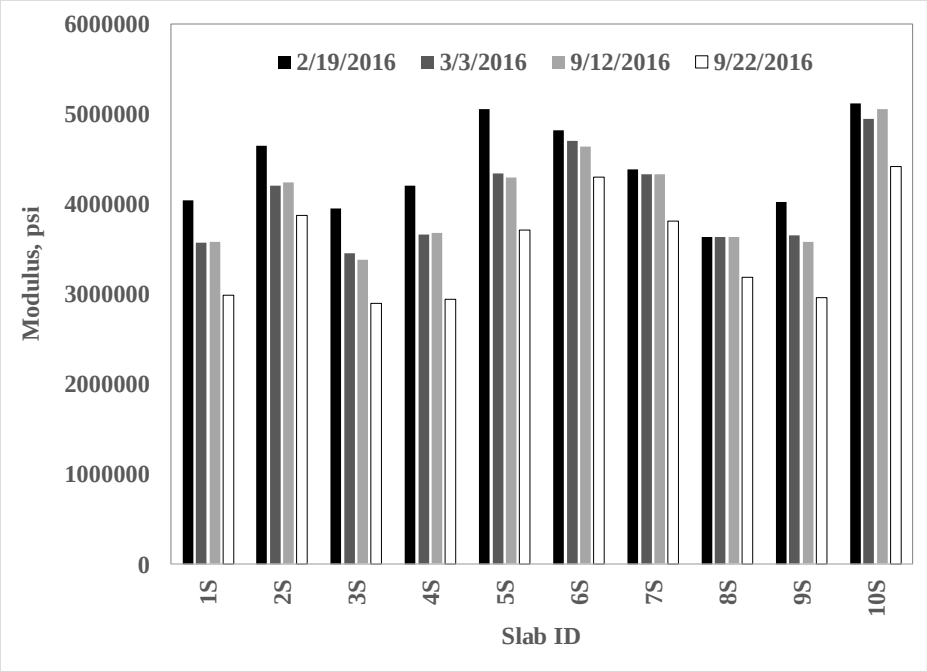

(a) Concrete

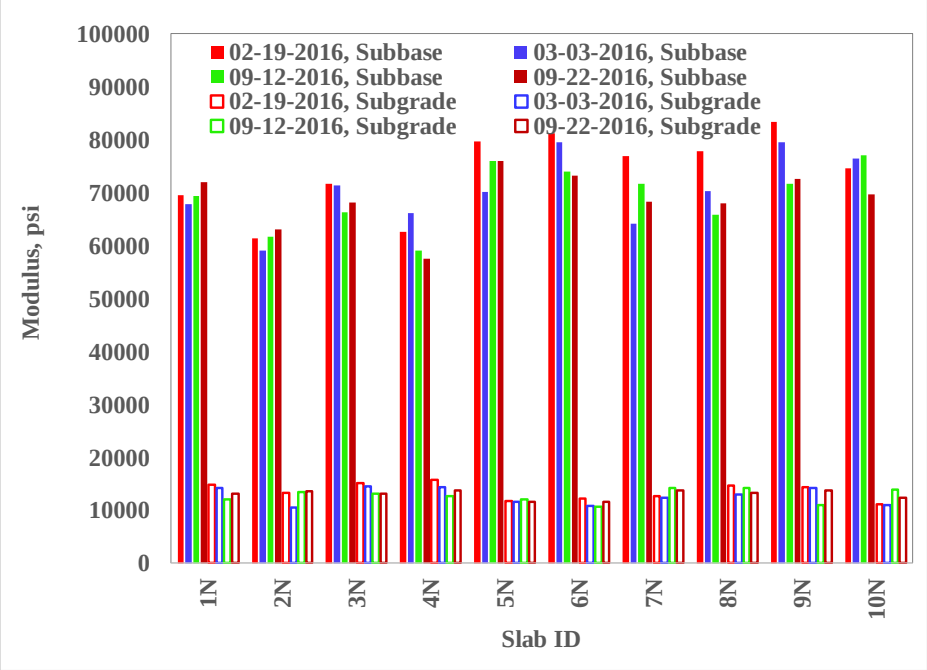

(b) Subbase and subgrade

Figure 17. Backcalculated Layer Moduli Over Time, North Test Item.

11. INSTRUMENTATION RESPONSE ANALYSIS

Embedded strain gage (EG), potentiometer (POT), and Eddy Current Sensor (ECS) data were collected through the SPUs during traffic test. The temperature and moisture data, which are

entirely static (not load-dependent), were collected hourly so that environmental changes could be monitored. The data analysis of potentiometers and moisture sensors are not included in this report.

12. CONCRETE TEMPERATURE

Concrete temperatures were monitored by the thermocouples installed at three depths in the P-501 layer: bottom, middle, and surface. As shown in figure 18a, the highest concrete temperature was recorded about 20 hours after pouring, 111^{o}F (figure 18b). Afterwards, the slab temperature started to drop due to the reduction of the heat from hydration. The temperature became stable after two days. In field, the surface temperature is strongly influenced by solar radiation, air temperature, wind speed, and to some extent, the temperature of the ground. However, due to NAPTF's indoor environment, none of these factors affected the pavement temperature and a constant temperature fluctuation of 5-10^{o}F over each 24-hr period was observed. Figures 18c and 18d plot the concrete temperature variations through the course of traffic testing. During the day, the upper portion of slab is always warmer. During the night, the temperature distribution in the slab is more uniform. During the transition period between day and night, the temperatures at different depths were equal to one another. Assuming a linear interpolation between the bottom and surface temperatures, the maximum thermal gradient of 0.28^{o}F/in was recorded at 14:00, 03/01/2016.

13. EMBEDDED STRAIN GAGE

Prior to the traffic testing, two loading passes were applied with a dual (D) gear configuration at 10,000 lbs. per wheel. These slow-roll passes (0.5 mph) were for the purpose of checking strain gage responses and were conducted only on four tracks as shown in figure 3: -4, -1, 0, 4. For the south test item, it was found that EG-S-O-I-3 registered the maximum tensile strain at the slab surface under Track -4 and EG-S-O-I-8 registered the maximum tensile strain at the bottom of the slab under Track 0. For the north test item, EG-N-O-I-1 registered the maximum tensile strain at the slab surface under Track -1 and EG-N-O-I-8 registered the maximum tensile strain at the bottom of the slab under Track 0. These four gages were therefore selected to monitor pavement responses during the traffic test, thereby maximizing the opportunity of capturing both top-down and bottom-up crack initiation.

For demonstration purpose, sample strain responses from EG-S-O-I-3 and EG-S-O-I-8 during normal traffic and initial overload test are provided in figures 19a and 19b, respectively. Along the transverse joint, EG-S-O-I-3 experienced slab surface tension only. The longitudinal strain gage (EG-S-O-I-8) recorded a counter-strain as the load approached and another strain reversal as the load left. Note that the steep post-peak strain recovery was a result of the formation of transverse joint at STA 3+54 (figure 19b). In addition, the peak strains did not vary with the passage of each subsequent axle. Compared to the normal traffic, the overloads induced a higher peak tensile strain at the slab surface and smaller peak tensile strains at the bottom of the slab. This observation agrees with the previous findings at the NAPTF that the tensile stresses developed at the slab bottom were related primarily to the wheel load, while the tensile stresses on the slab surface were related primarily to the gear load at both the longitudinal and transverse joint locations (Brill 2011).

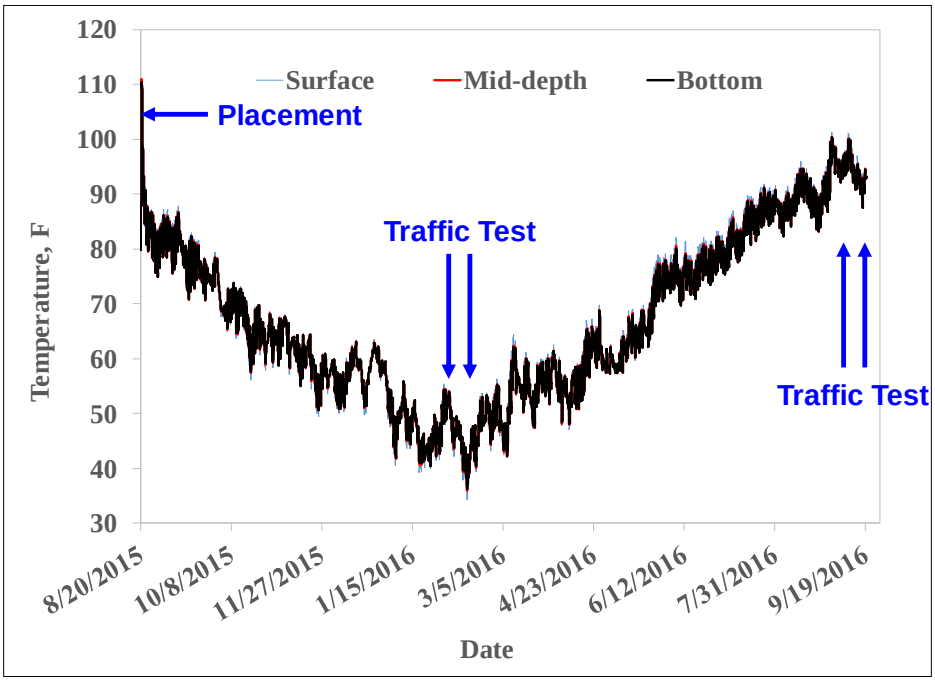

(a) 08/20/2015 – 09/19/2016

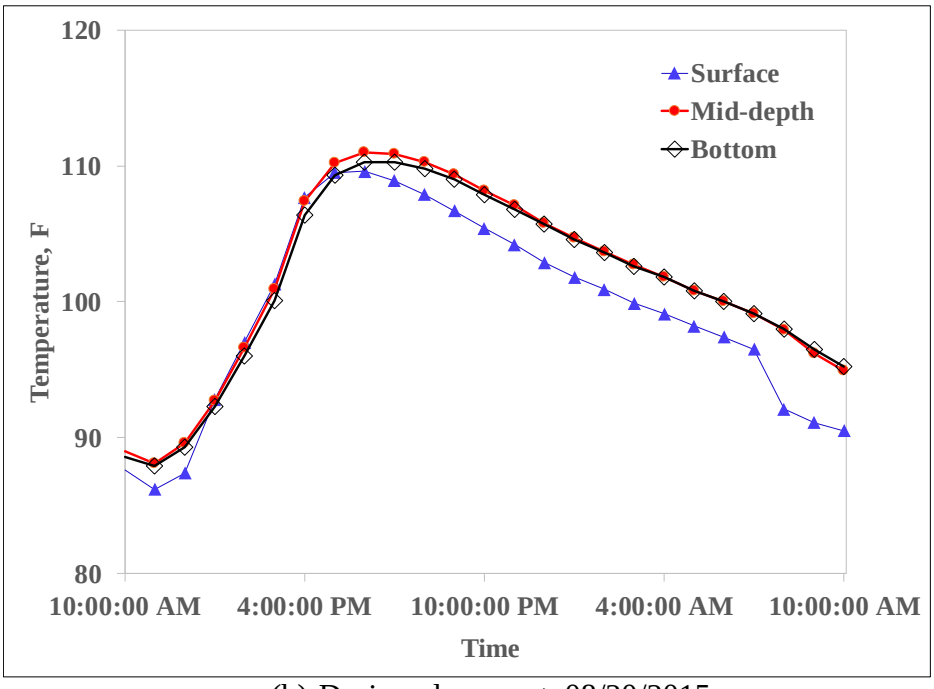

(b) During placement, 08/20/2015

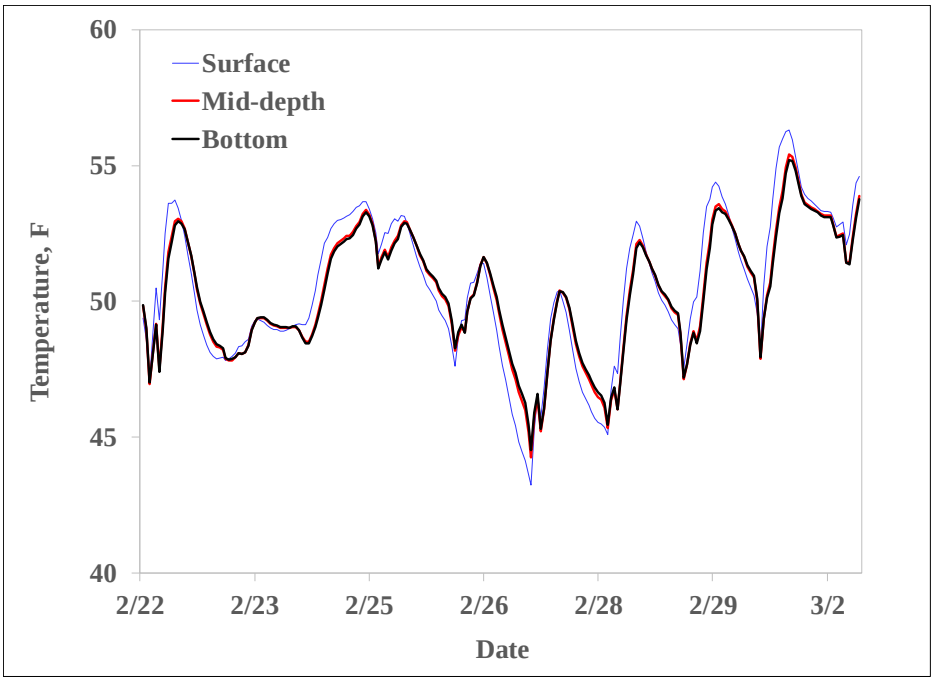

(c) 02/22/2016 – 03/02/2016

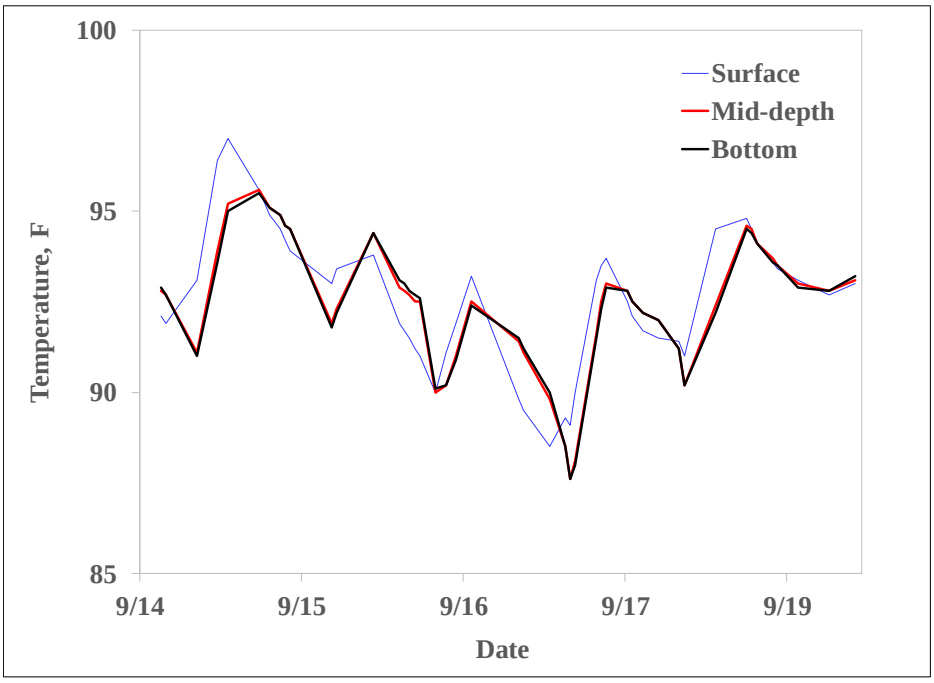

(d) 09/14/2016 – 09/19/2016

Figure 18. Concrete Temperature.

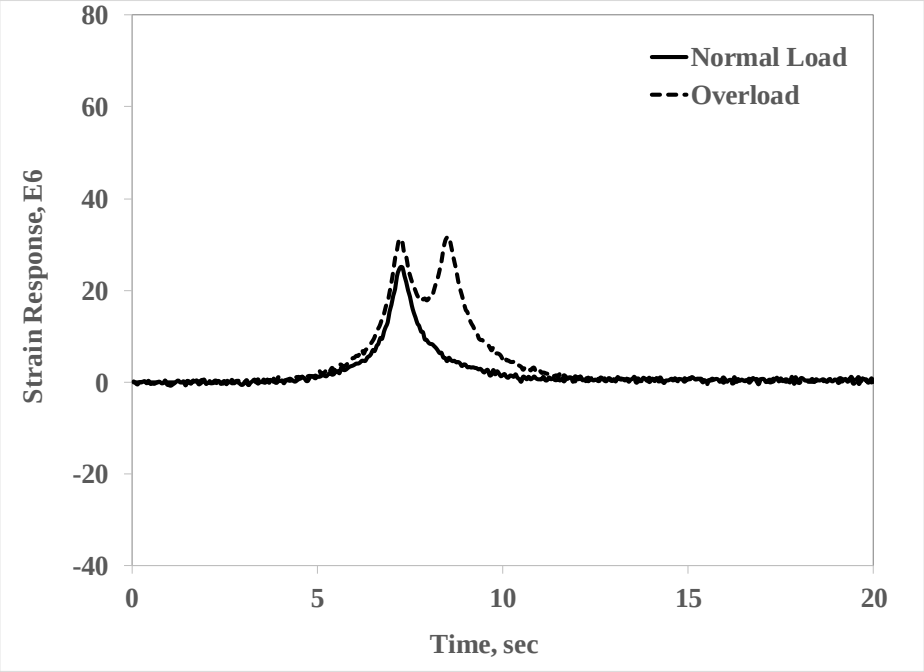

(a) EG-S-O-I-3

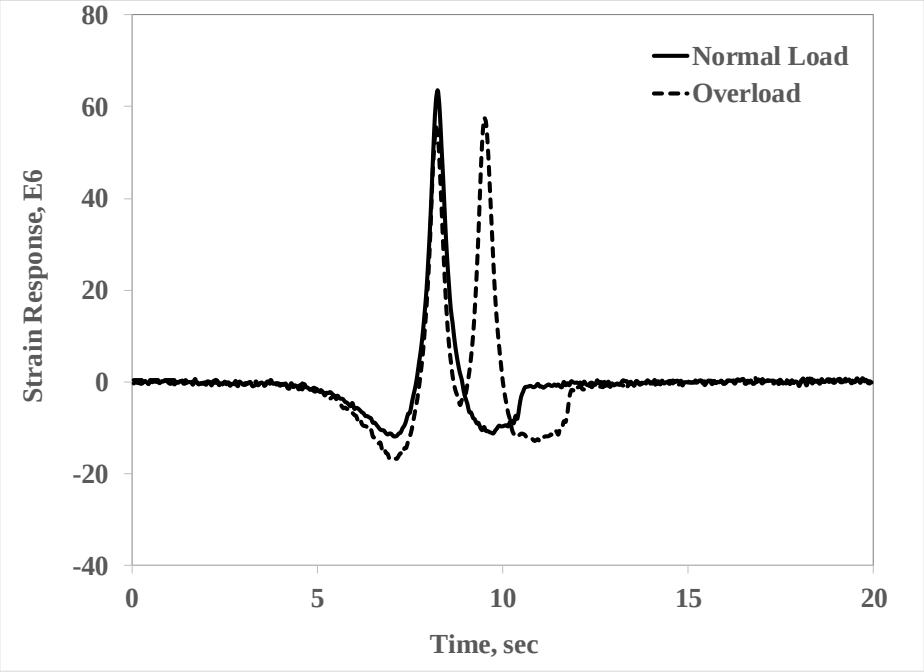

(b) EG-S-O-I-8

Figure 19. Sample Embedded Strain Gage Responses.

Figure 20 contains a history plot of peak tensile strains from all four monitoring embedded strain gages. For the south test item, the tensile strains at the slab bottom were always higher than those on the surface. Neither of the gage responses indicated a crack initiation. After a quick recovery from the peak response of 40 microstrains under the highest overload, the tensile strains from transverse gage (EG-S-O-I-3) remained steady at 30 microstrains till the end of traffic

testing, indicating no load-induced damage close to the slab surface. On the other hand, a gradual decline in strain was registered by EG-S-O-I-8 at the slab bottom along the longitudinal joint. For the north test item, the initial tensile strains at the slab bottom were much higher than those on the surface. Then the bottom strains steadily decreased and the surface strains increased, and eventually crossed each other after 4000 passes. There was also a distinct jump in the responses due to the increase of wheel load from 20,000 lbs to 28,000 lbs. The maximum bottom tensile strain was about 80 and 70 microstrains for the south and north test item, respectively. The application of overloads seemed to have a minimal effect in strain responses.

14. ESC DEFLECTION SENSOR

Deflections at the west corners of Slab 3S and 8S were measured by ECS. Two ECS sensors were installed on a trial basis on the south test item only. The ECS sensors performed well and will be used more extensively in the second phase of CC8 and in future applications. Referring to the ECS locations in figure 1, and the wander pattern in figure 3, the maximum deflections were recorded on Track 1 for ECS-S-O-I-1 and on Track 0 for ECS-S-O-I-2. For those particular wander positions, one wheel passes directly over the slab corner associated with the sensor. Sample deflection responses are presented in figures 21a and 21b. As the wheel approached the transverse joint, the deflection sensor on the opposite slab recorded an upward deflection followed by an abrupt downward movement as the wheel crossed the joint. The peak negative response corresponds to the wheel position directly above the slab corner. The load-inducted deflections gradually recovered as the wheel left the slab. The magnitude of peak deflections depends not only on the wheel load, but also on the gear configuration. In contrast to the full deflection recovery under D gear loads (normal loads), there was some upward residual deflection (negative rebound) observed after each 2D (overload) gear passage, perhaps resulting from the partial recovery between axles. For both normal traffic and overloads, ECS-S-O-I-1 recorded somewhat higher peak deflections, indicating a slightly lower level of support under the west corner of Slab 3S, compared with Slab 8S. Nevertheless, the deflections recorded by the two sensors under equal loads are very similar.

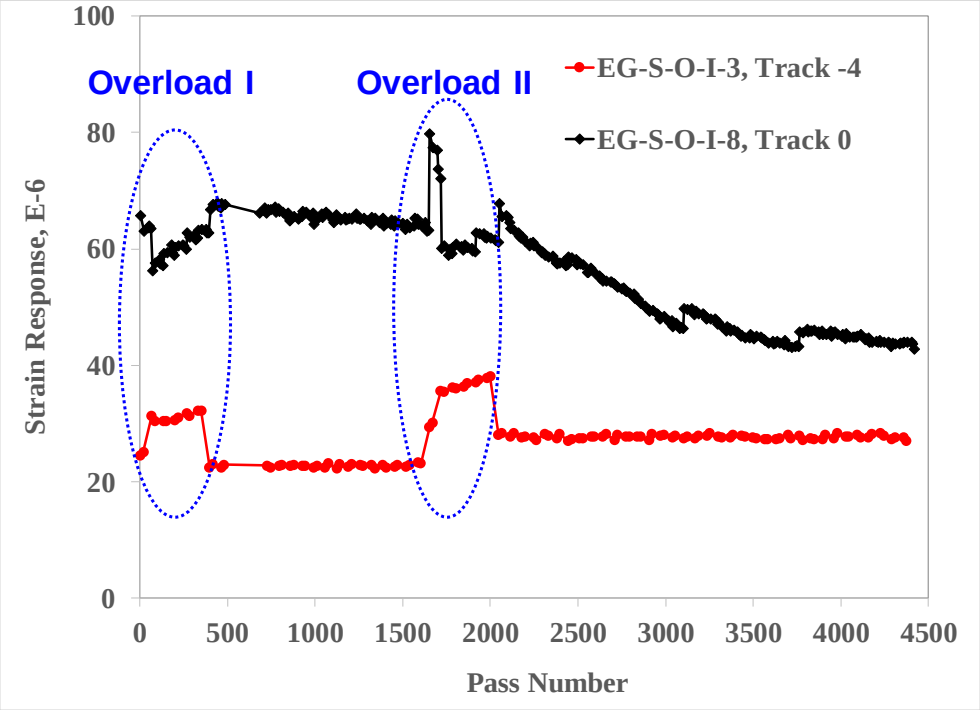

(a) South

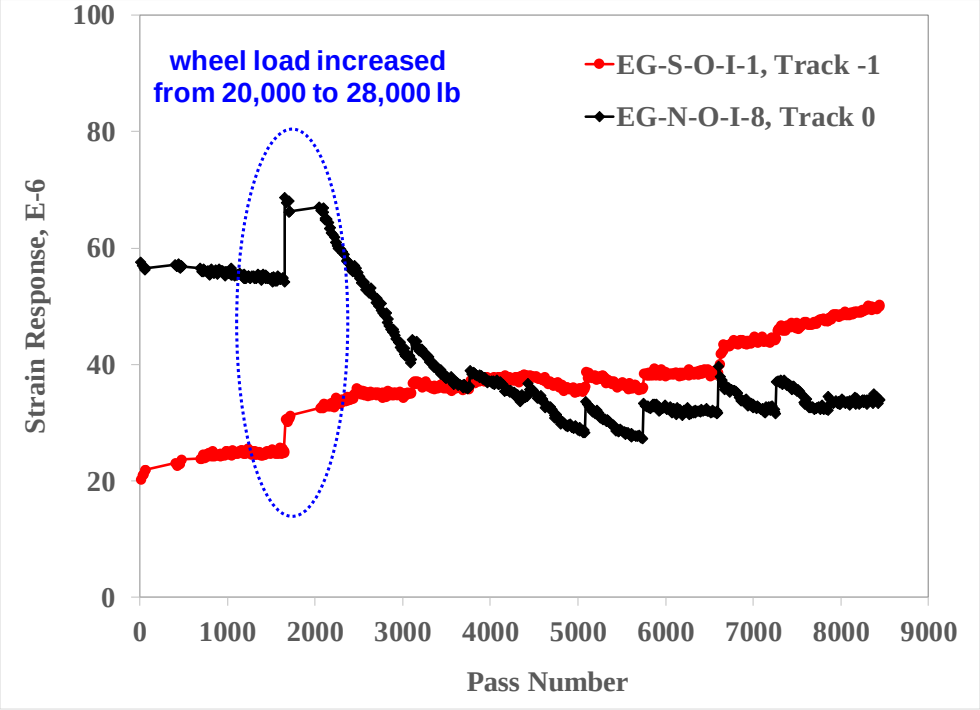

(b) North

Figure 20. Strain Response History.

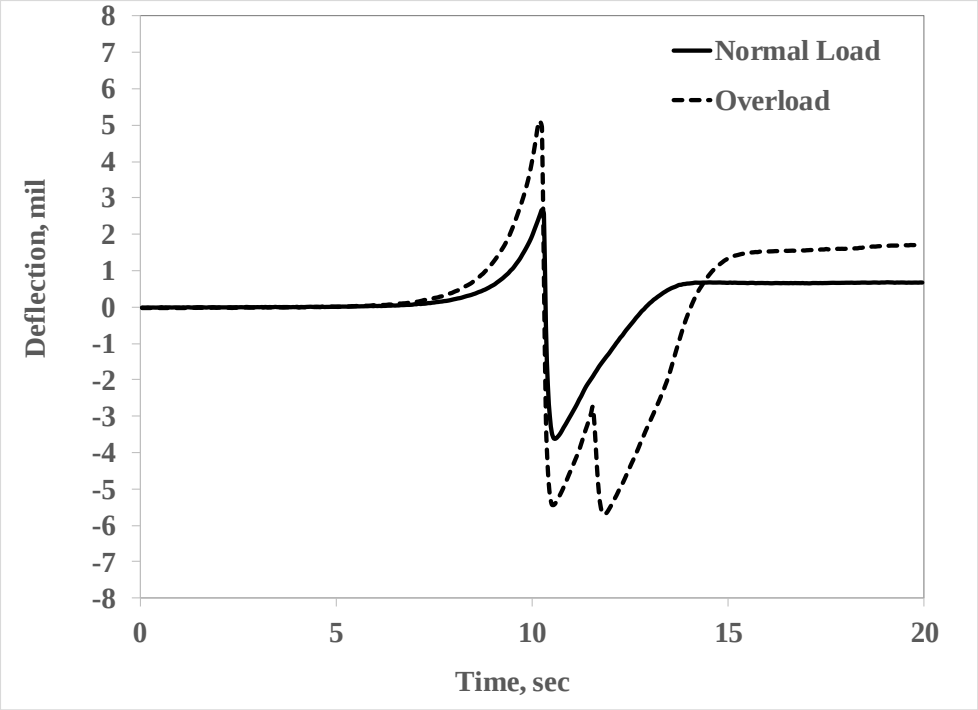

(a) ECS-S-O-I-1

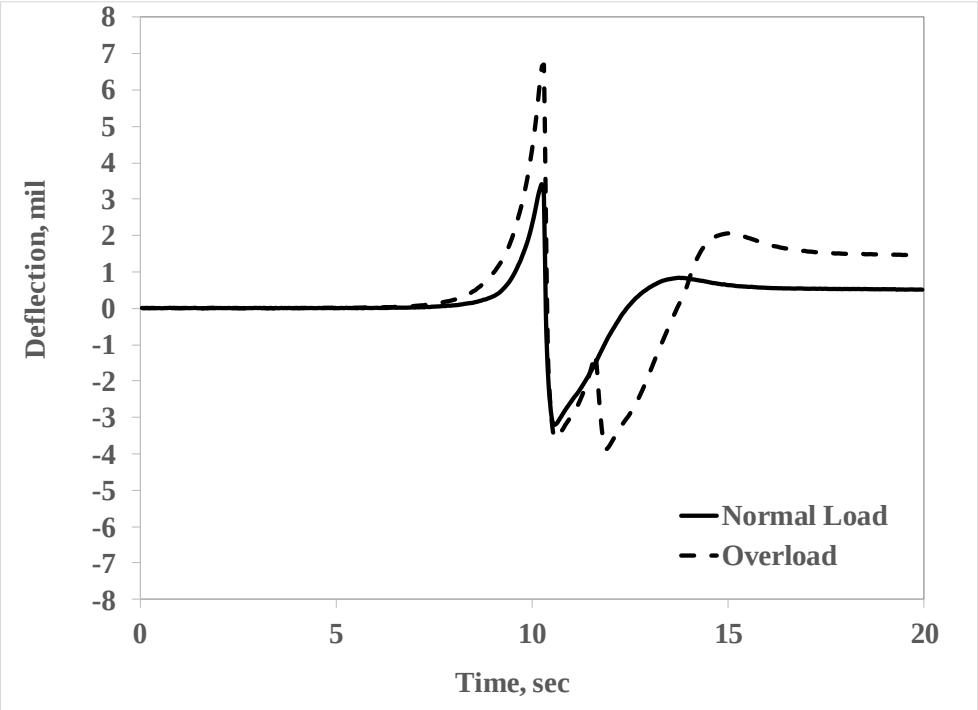

(b) ECS-S-O-I-2

Figure 21. Deflection Sensor Responses.

In Figure 22, peak deflections from ECS-S-O-I-1 and ECS-S-O-I-2 are plotted against accumulated load passes. In this plot, positive deflections are downward. In both cases, peak downward deflections at slab corners increased rapidly under the overload traffic, then gradually recovered under subsequent normal traffic. An interesting observation concerns behavior during overnight rest periods. When the traffic test resumed in the morning (approximately 7:30 am), there was always an increase in deflection compared to the end of traffic on the previous day, which was attributed to the upward movement in the slab during the night. At failure, there was a sudden drop in peak deflection response (over 20 mils), suggesting that the developing cracks had destroyed the slab flexure completely. Corresponding to this change, after 4,158 total passes, cracks became visible on the surface of Slabs 3S and 8S.

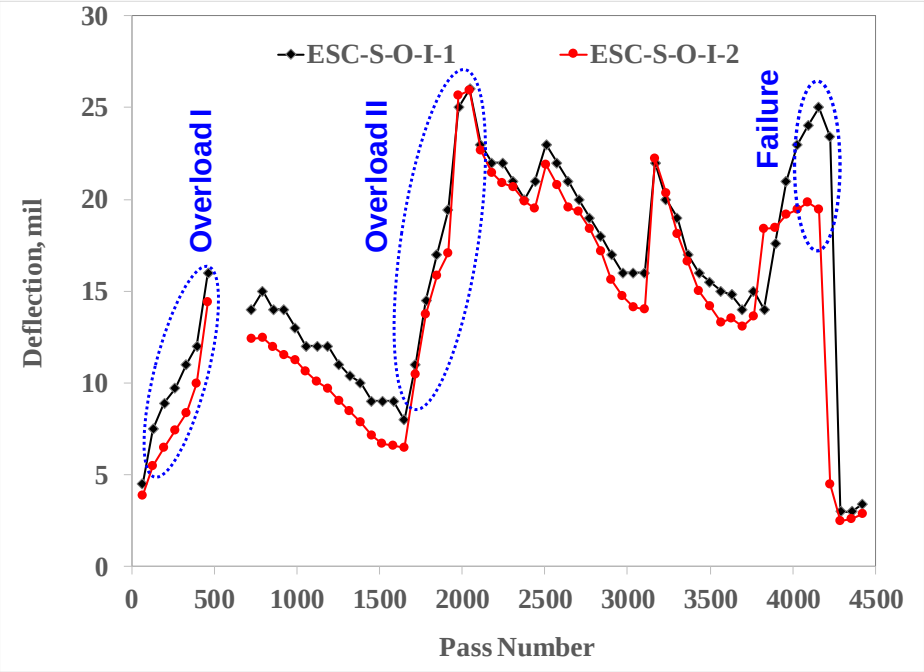

Figure 22. Deflection Sensor Response History.

To further examine the failure at slab corners, deflection responses were extracted from different phases of traffic and a comparison of these responses is presented in figure 23. It is clear that the total load-induced corner deflection was a combination of the downward movement under the loads and the upward residual movement following the loads. The ratio between these two opposite movements was controlled by the wheel load. During the second overload traffic, the contribution from the residual deflections was as high as 25 percent of the peak deflections. A reasonable conclusion is that the overloads formed voids under slab corners, produced negative rebound along the outer edge of the slab, and eventually initiated cracks on the surface.

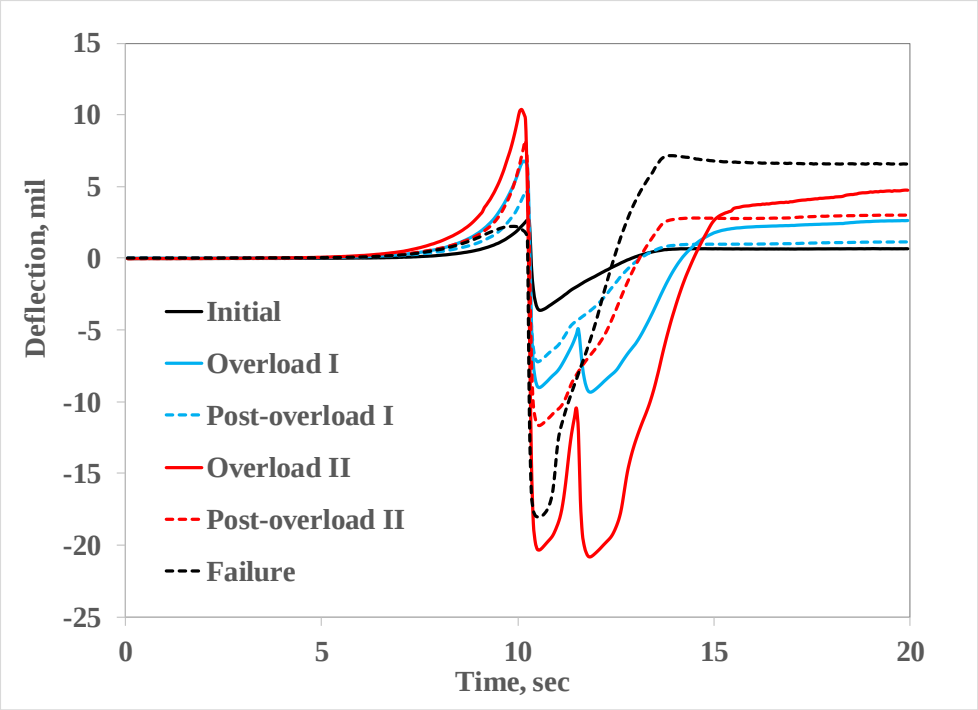

(a) ECS-S-O-I-1

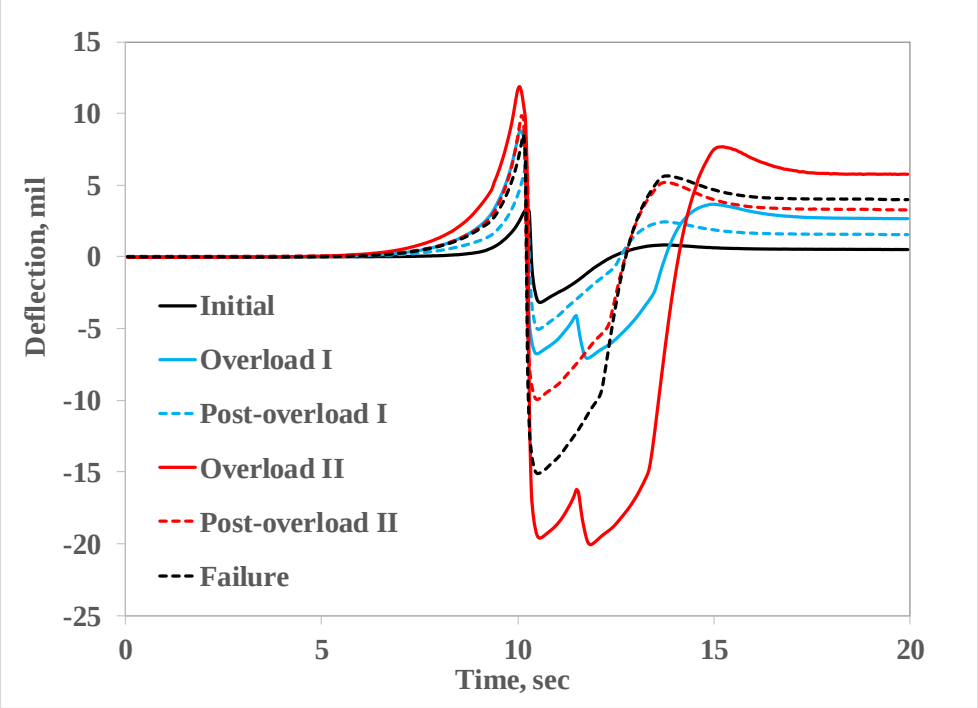

(b) ECS-S-O-I-2

Figure 23. Deflection Responses Extracted from Different Testing Periods.

15. FAILURE MECHANISM

The observed distresses are the result of wheel load repetitions at slab corners that cause corner deflections and stresses in the top surface of the slab, resulting in fatigue damage and ultimate cracking. It is important to note that the top-down cracks did not occur under the action of the overloads themselves; rather, the overloads provided the opportunity for fatigue damage to take place earlier than it would otherwise. The magnitude and frequency of loads, the support conditions at slab corners, the uniformity of the subbase, and the degree of joint load transfer, all combine to permit excessive downward corner deflections. As the corner becomes progressively less supported and experiences correspondingly higher deflections and stresses under loads, distresses occur along the outer edge of the slab. A graphic demonstration of such localized failure is given in figure 12. Hypothetically, a stronger support from underlying layers (e.g., stabilized subbase) would provide protection against the observed distresses at slab corners.

Airfield rigid pavement thickness design has traditionally been based on the critical tensile bending stress at the bottom of the slab. Recent observations from Construction Cycle 6 (CC6) traffic tests at the FAA NAPTF have shown top-down cracking can occur under certain combined loading and pavement geometry situations (Brill and Kawa 2014). In addition, full-scale testing at the NAPTF has demonstrated that top-down cracks progress from initiation to full depth much more quickly than bottom-up cracks. The current FAARFIELD thickness design procedure does not consider this failure mode (FAA 2009). Instead, current FAA standards attempt to limit top-down cracks through joint spacing limitations based on experience and rules-of-thumb. As summarized in *Operational Life of Airport Pavements* (Garg et al. 2004), top-down cracking is typically expected in larger slabs and when curling is significant, and is also expected to appear in the form of corner breaks. A similar cracking pattern was observed during previous accelerated testing, and the causes have been thoroughly examined but not yet fully explained using finite element analysis (Evangelista and Roesler 2009). Small airports sometimes require accommodating a limited number of operations of an airplane heavier than the pavement was designed to support. For these thinner concrete slabs, the risk of top-down cracking becomes a major concern for allowing or rejecting the overload operations. In addition, field survey data for medium and large airports suggests that top-down cracks have to be considered for terminal pavements where heavy airplanes irregularly move near the slab corners (FAA 2013).

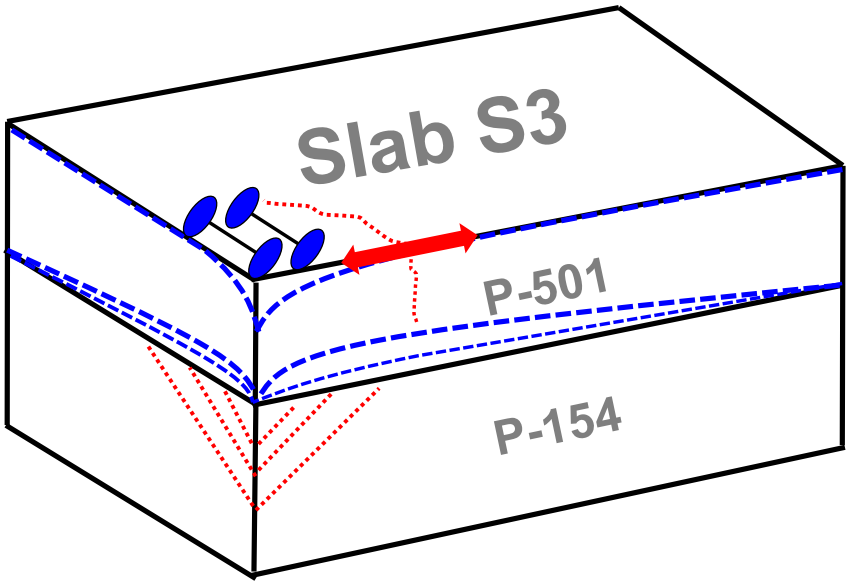

Figure 24. Failure Mechanism.

16. OVERLOAD EFFECTS

As shown in table 2, at the end of traffic testing, two test items not only experienced different traffic pass totals (4422 versus 7788) but also were subjected to mixed aircraft traffic. The reason for using different load levels was the necessity of failing the test pavement within a reasonable period of time. Figure 25 shows the raw data of SCI versus cumulative traffic passes for the north and south test item, unadjusted for load. The departure of the curves from the SCI = 100 portion would approximately represent the onset of structural deterioration. However, it may take some time to visually observe a crack.

To reasonably compare the performance of different test items in a meaningful way, an analytical procedure (Brill and Kawa 2014) was adopted here to compensate for different load levels. The first step was to determine the number of traffic passes to failure. In this analysis, for purposes of comparison between test items, the failure condition was selected at SCI 80. As shown in figure 25, the total number of passes to SCI 80 were obtained by linear regression through the semi-log plots of SCI versus passes: 7582 for the north and 4156 for the south.

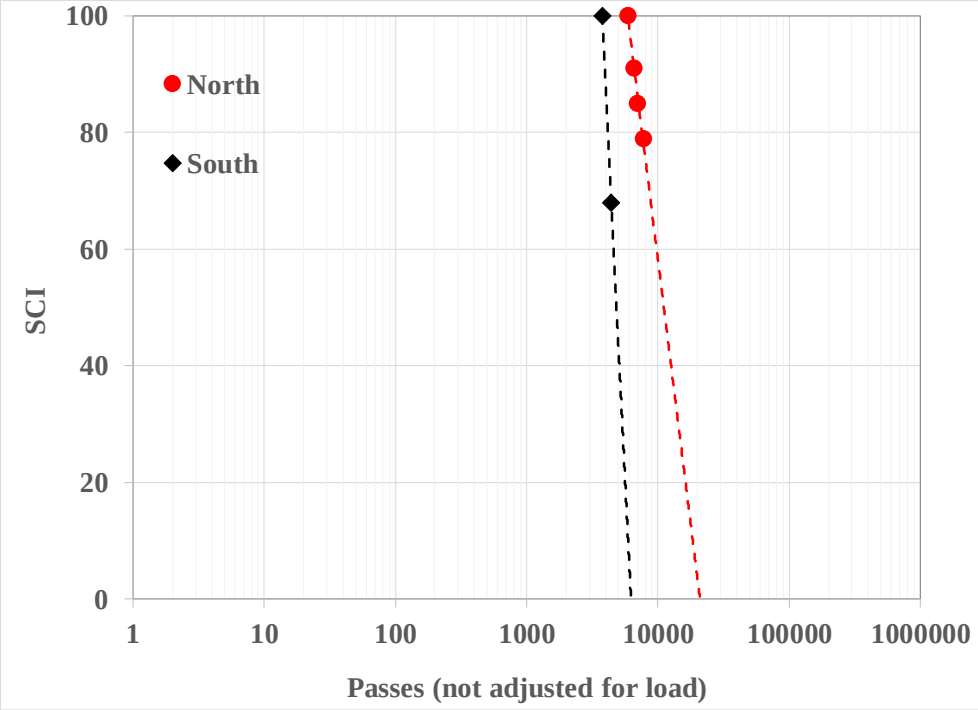

Figure 25. SCI as a Function of Traffic Passes.

Next, the FAA pavement thickness design program FAARFIELD was used to compute the pass/coverage ratio and then convert traffic passes to coverages (figure 26). As summarized in table 4, a total of 1300 and 697 coverages were required for the north and south test item to reach the same failure condition, respectively. Stresses in table 4 are the maximum concrete bending stresses computed by FAARFIELD, version 1.4. Note that all inputs were the same for both test items except for the k-value of subgrade: 131 pci for the north and 110 pci for the south.

For mixed aircraft traffic, the cumulative damage factor (CDF) is expressed as:

$$CDF = \sum_{i=1}^{N} \frac{C_i}{C_{Fi}} \quad (7)$$

Where:
Ci = the actual number of coverages for aircraft i
CF_i = the number of coverages to failure for aircraft i
N= the number of aircraft considered (2 for north and 14 for south)

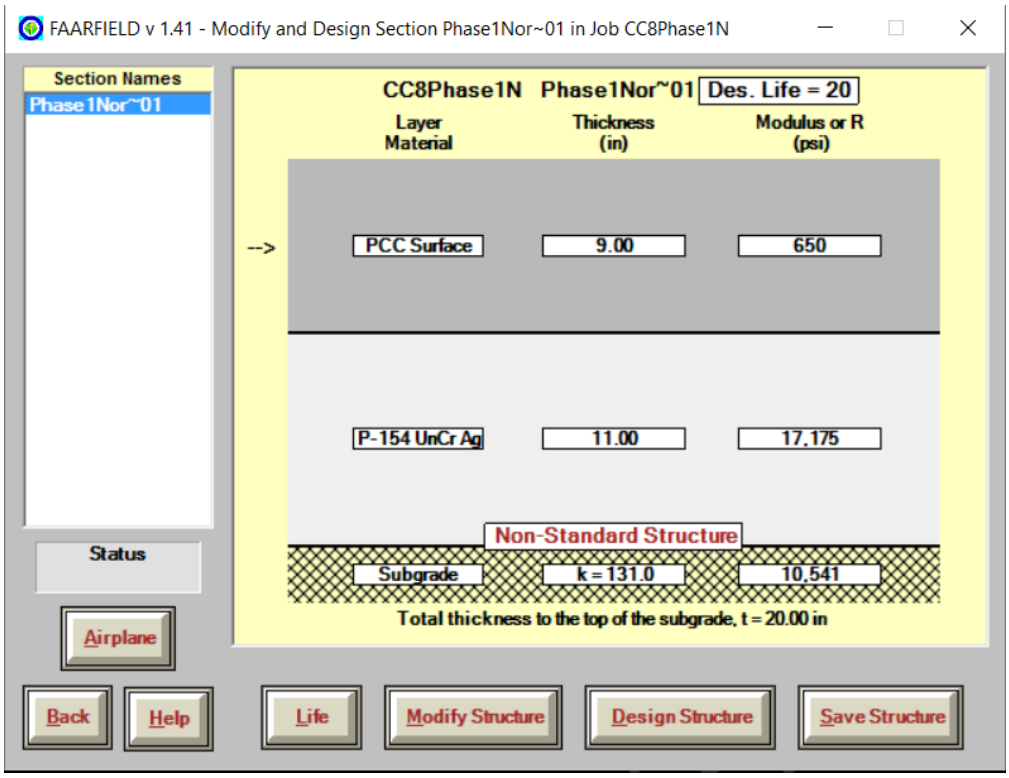

(a) North

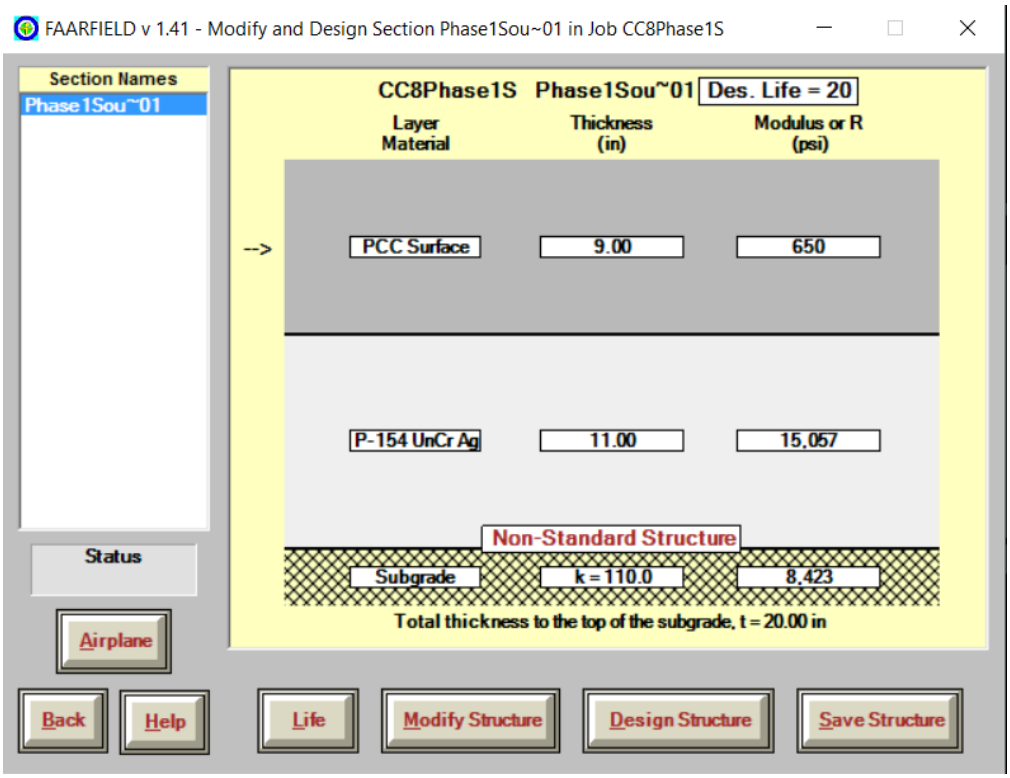

(b) South

Figure 26. FAARFIELD 1.4 Comparative Life Computations.

Using Equation 8, the data in table 4 may be fitted to the rigid failure model in FAARFIELD:

$$C_F = A \times 10^{B(\frac{R}{\sigma})} \quad (8)$$

Where:
CF = coverages to failure (SCI 80)
R = concrete flexural strength
σ = computed slab stress
A and B = model coefficient

For a given traffic mix known to cause failure, the model coefficients A and B in Equation 8 can be estimated assuming the pavement failure occurs and CDF = 1. Substituting R = 650 psi and coverages (C1 - C2 for the north, and C1 - C14 for the south) from table 4, the following estimates were obtained:

- North: A = 0.125, B = 4.558
- South: A = 0.102, B = 4.380

The last step was to calculate the equivalent number of coverages of the trafficking gear at a reference wheel load that would cause failure. For this analysis, a reference wheel load of 20,000 lbs was selected. This was done by holding previously estimated A and B, substituting σ = 578 psi (north) and 608 psi (south) for the stress value in each term of Equation 8, and adjusting the number of coverages until the value of each term matched previous values (CDF = 1). The equivalent passes to failure for both north and south test item at the reference load level (20,000 lbs) are listed in table 4. It is clear from table 4 that when compared on the basis of equivalent coverages at a reference load, the overloaded test item (south) had a much shorter pavement fatigue life than the normal loaded test item (north).

The failure model in FAARFIELD assumes that the SCI deteriorates under traffic as a linear function of the logarithm of coverages (after first reaching the first structural crack). To further examine the structural deterioration under overloads, the above analytical procedure was repeated to determine equivalent coverages at the second failure condition (SCI 90) such that a failure curve can be established. The equivalent number of coverages of the trafficking gear at the same reference wheel load, 20,000 lbs, are listed in the last column of table 4.

Table 5. Calculation of Equivalent Coverages to Failure (SCI 80 and SCI 90).

North										
Gear Configuration	Wheel Load, lbs	Passes	Stress, psi	Pass/Coverage	SCI 80			SCI 90		
					Coverages		Equivalent Coverages	Coverages		Equivalent Coverages
D	20000	1716	578	6.66	C1	258	258	C1	258	258
D	28000	5866	745	5.63	C2	1042	16368	C2	881	14482
Total		7582				1300	16626		1139	14740
South										
Gear Configuration	Wheel Load, lbs	Passes	Stress, psi	Pass/Coverage	SCI 80			SCI 90		
					Coverages		Equivalent Coverages	Coverages		Equivalent Coverages
D	20000	66	608	6.66	C1	10	10	C1	10	10
2D	21500	66	529	6.42	C2	10	2	C2	10	2
2D	22500	66	548	6.28	C3	11	4	C3	11	4
2D	23000	66	558	6.21	C4	11	5	C4	11	5
2D	24000	66	577	6.08	C5	11	6	C5	11	6
2D	25000	66	597	5.96	C6	11	9	C6	11	9
D	20000	1320	608	6.66	C7	198	198	C7	198	198
D	28000	66	787	5.63	C8	12	140	C8	12	137
2D	28500	66	663	5.58	C9	12	30	C9	12	29
2D	29500	66	682	5.48	C10	12	39	C10	12	38
2D	30500	66	701	5.39	C11	12	50	C11	12	50
2D	31500	66	720	5.31	C12	12	64	C12	12	64
2D	32500	66	738	5.23	C13	13	87	C13	13	85
D	28000	2044	787	5.63	C14	363	4250	C14	327	3743
Total		4156				697	4891		661	4379

In figure 27, the structural deterioration for both test items are plotted versus cumulative coverages on a logarithmic scale to correspond to traditional plotting of fatigue relationships. This performance curve is a key product of this research effort, and two important observations can be obtained from it. At the same reference load level, overloads considerably shortened pavement fatigue life up to the first full-depth crack (i.e., at which SCI just begins to diminish from its initial level of 100). In addition, figure 27 suggests that overloads did not affect the rate of structural deterioration (slope of the falling leg of the SCI-vs-log(C) curve).

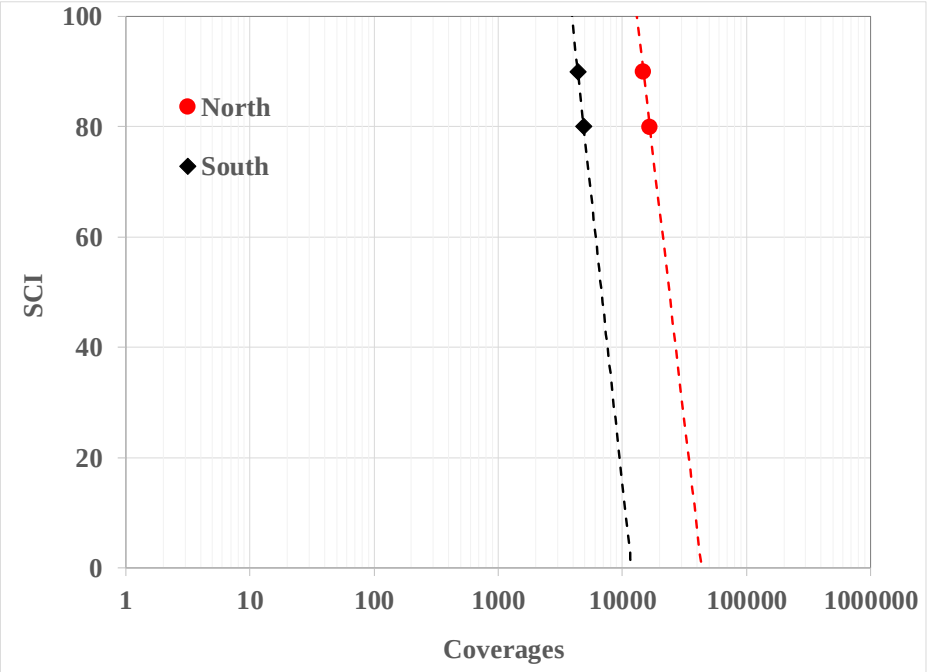

Figure 27. SCI as a Function of Coverages.

17. CONCLUSIONS

To evaluate the ICAO overload criteria for rigid pavements, a concrete pavement was constructed, instrumented, and tested at the FAA NAPTF. The test pavement consisted of 9-inch thick PCC surface layer and 11-inch thick aggregate subbase on a processed clay subgrade. Traffic testing began in February 2016 and ended in September 2016. This report provides details of the overload experiment. Key findings are:

- The observed distresses are the result of wheel load repetitions at slab corners causing corner deflections and stresses in the top surface of the slab, resulting in fatigue damage and ultimate cracking.
- The fatigue failure of the overloaded slabs was accelerated because heavy wheel loads compressed the aggregate base, thereby opening a void space under the slab and providing the opportunity for top-down cracking. These results suggest that the use of stabilized bases under rigid pavements may provide benefit in the form of additional tolerance of occasional overloads, i.e., beyond the limit currently established by ICAO (5% above PCN for rigid pavements).

- Overloads considerably shortened pavement fatigue life up to the first full-depth crack (i.e., at which SCI just begins to diminish from its initial level of 100).
- Overloads did not affect the rate of structural deterioration (slope of the falling leg of the SCI-vs-log(C) curve).

CC8 Phase I test generated a unique full-scale test data set, which will be of immediate interest to airport operations.

18. REFERENCES

1. American Association of State Highway and Transportation Officials. *AASHTO Guide for Design of Pavement Structure*, 1993.
2. ASTM. "Standard Test Method for Compressive Strength of Cylindrical Concrete Specimens." C39-05, American Standard for Test and Materials, West Conshohocken, PA, 2005.
3. ASTM. "Standard Test Method for Flexural Strength of Concrete (Using Simple Beam with Third-Point Loading)," C78-07, American Standard for Test and Materials, West Conshohocken, PA, 2007.
4. ASTM. "Standard Test Method for Airport Pavement Condition Index Surveys," D5340-12, American Standard for Test and Materials, West Conshohocken, PA, 2012.
5. Brill, D.R. "Review of 10 Years of Concrete Airport Pavement Studies at the NAPTF and Next 10 Year Plan," *2nd International Conference on the Best Practices for Concrete Pavements*, Florianopolis, Brazil, 2011.
6. Brill, D.R. and Kawa, I. "Relative Performance of CC6 Concrete Pavement Test Items at the FAA National Airport Pavement Test Facility," *XL ALACPA Seminar on Airport Pavements and IX FAA Workshop*, Santiago, Chile, 2014.
7. Brill, D.R. and Kawa, I. "Relative Performance of CC6 Concrete Pavement Test Items at the FAA National Airport Pavement Test Facility," *FAA Worldwide Airport Technology Transfer Conference.*
8. Defence Estates. (2011). UK Ministry of Defence. *A Guide to Airfield Pavement Design and Evaluation, Design and Maintenance Guide 27, 3rd Edition.*
9. Evangelista, J.F. and Roesler, J.R. "Top Down Cracking Predictions for Airfield Rigid Pavements," *Transportation Research Board, Issue No. 2095, 2009*.
10. Federal Aviation Administration. *AC 150/5320-6E, Airport Pavement Design and Evaluation*, 2009.
11. Federal Aviation Administration. *AC 150/5370-11A, Use of Nondestructive Testing in the Evaluation of Airport Pavements*, 2011.
12. Federal Aviation Administration. *Airport Pavement 10-year R&D Program, Airport Pavement Design and Evaluation*, 2013.
13. Garg, N., Guo, E. and McQueen, R. "Operational Life of Airport Pavements," Technical Report No. DOT/FAA/AR-04/46, Federal Aviation Administration, Office of Aviation Research, 2004.
14. Nazarian, S., Yuan, D., Smith, K., Ansari, F., and Gonzalez, C. "Acceptance Criteria of Airfield Concrete Pavement Using Seismic and Maturity Concepts," Innovative Pavement Research Foundation (IPRF) Project IPRF-01-G-002-02-2, 2006.

15. Yin, H. “Construction Cycle 8 (CC8) Objectives, Concept Design, and Instrumentation,” 2013.